



**NUMERICAL ANALYSIS OF NANO-FLUID FLOW AND HEAT TRANSFER  
IN DUCTS**

**HUSSEIN R. ABDULHADI AL-TAMEEMI**

**JANUARY 2019**

NUMERICAL ANALYSIS OF NANO-FLUID FLOW AND HEAT TRANSFER IN  
DUCTS

A THESIS SUBMITTED TO  
THE GRADUATE SCHOOL OF NATURAL AND APPLIED SCIENCES  
OF ÇANKAYA UNIVERSITY

BY

HUSSEIN R. ABDULHADI AL-TAMEEMI

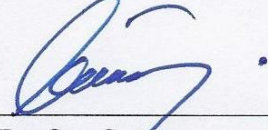
IN PARTIAL FULFILLMENT OF THE REQUIREMENTS FOR THE  
DEGREE OF  
MASTER OF SCIENCE  
IN  
MECHANICAL ENGINEERING

JANUARY 2019

Approval of the Thesis: **NUMERICAL ANALYSIS OF NANO-FLUID FLOW AND HEAT TRANSFER IN DUCTS**

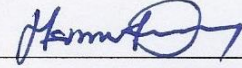
Submitted by **HUSSEIN R. ABDULHADI AL-TAMEEMI**

Approval of the Graduate School of Natural and Applied Sciences, Çankaya University



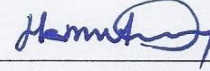
Prof. Dr. Can Çoğun  
Director

I certify that this thesis satisfies all the requirements as a thesis for the degree of Master of Science.



Prof. Dr. Haşmet Türkoğlu  
Head of Department

This is to certify that we have read this thesis and that in our opinion it is fully adequate, in scope and quality, as a thesis for the degree of Master of Science.



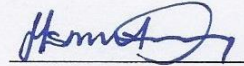
Prof. Dr. Haşmet Türkoğlu  
Supervisor

**Examination Date: 21. 01. 2019**

**Examining Committee Members**

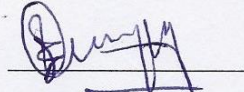
Prof. Dr. Haşmet Türkoğlu

(Çankaya University)



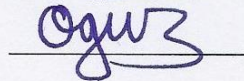
Asst. Prof. Dr. Ece Aylı

(Çankaya University)



Assoc. Prof. Dr. Oğuz Turgut

(Gazi University)

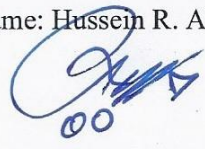


## STATEMENT OF NON-PLAGIARISM

I confirm that all information provided in this thesis is taken and presented according to the academic and ethical conduct which requires the referencing and citation of any material that are not original of this thesis.

Name, Last Name: Hussein R. Abdulhadi AL-TAMEEMI

Signature:

A handwritten signature in blue ink, appearing to be 'Hussein R. Abdulhadi AL-TAMEEMI', with the initials '00' written below it.

Date:

31/01/2019

## ABSTRACT

# NUMERICAL ANALYSIS OF NANO-FLUID FLOW AND HEAT TRANSFER IN DUCTS

HUSSEIN R. ABDULHADI AL-TAMEEMI

M.S., Department of Mechanical Engineering

Supervisor: Prof. Dr. Haşmet TÜRKOĞLU

January 2019, 61 pages

In this study, turbulent nanofluid flow and heat transfer in a square duct with constant heat flux at the top and bottom surfaces and insulated front and back faces were investigated numerically. Fluent was used for the numerical solution of the governing equations of the problem. To model the turbulence, realizable k- $\epsilon$  model is used. The finite volume method (FVM) was used to discretize the continuity, momentum and energy equations. Three different types of nanoparticles  $\text{Al}_2\text{O}_3$ , ZnO, and CuO with different diameters (30, 29, 29 nm) at different volume fractions (in the range of 1% to 4%) were considered. Effects of these parameters on heat transfer rate and flow characteristics in the Reynolds numbers range of 10000 to 35000 were studied. The results of the simulations show a good agreement with the existing experimental correlations. The numerical results show that  $\text{Al}_2\text{O}_3$ -water has the highest Nusselt number compared to other nanofluids considered while it has the lowest heat transfer coefficient due to low thermal conductivity. It was observed that the Nusselt number increases with the increase in the Reynolds number and the volume fraction of nanoparticles.

**Keywords:** Nanofluid, square duct, CFD, nanoparticle, numerical simulation.

## ÖZ

### KANALLARDA NANO AKIŞKAN AKIŞININ VE ISI TRANSFERİNİN SAYISAL OLARAK İNCELENMESİ

HUSSEIN R. ABDULHADI AL-TAMEEMI

Yüksek Lisans, Makine Mühendisliği Anabilim Dalı

Tez Yöneticisi: Prof. Dr. Haşmet TÜRKOĞLU

Ocak 2019, 61 sayfa

Bu çalışmada, kare kesitli bir kanalda türbülanslı nanoakışkan akışı ve ısı transfer sayısal olarak analiz edilmiştir. Kanalın alt ve üst yüzeylerine sabit ısı akısı uygulanmış, ön ve arka yüzeyler yalıtılmıştır. Problemin denklemlerini çözmek için FLUENT yazılımı kullanılmıştır. Süreklilik, momentum ve enerji denklemlerinin ayrıklaştırılmasında sonlu hacimler yöntemi (FVM) kullanıldı. Çalışmada, nanoakışkanların farklı hacim oranları (1% ve 4% aralığında), farklı nanoparçacık çaplı (30, 29, 29 nm) üç farklı tipte nanoparçacık ( $Al_2O_3$ , ZnO ve CuO) için simülasyonlar yapılmıştır. Reynolds sayısının 10000 ile 35000 aralığındaki değerleri için çözümler yapılarak bu parametrelerin akış ve ısı transferi üzerine etkisi incelenmiştir. Sayısal sonuçlar  $Al_2O_3$ -su karışımının diğer nanoakışkanlara göre en yüksek Nusselt sayısına sahip olduğunu göstermiştir. Ancak ısı iletim katsayısının küçük olmasında dolayı en düşük ısı transfer katsayısını vermiştir. Nusselt sayısı, Reynolds sayısı ve nanopartikül hacimsel oranı ile artmaktadır. Simülasyon sonuçları mevcut deneysel korelasyonlarla uyum içerisindedir.

**Anahtar Kelimeler:** Nanoakışkan, kare kanal, CFD, nanoparçacık, sayısal simülasyon.

## ACKNOWLEDGMENTS

I would like to express my special thanks of gratitude to Prof. Dr. Haşmet TÜRKOĞLU as well as our principal who gave me the golden opportunity to do this wonderful thesis on the topic “NUMERICAL ANALYSIS OF NANO-FLUID FLOW AND HEAT TRANSFER IN DUCTS”, which also helped me in doing a lot of research and I came to know about so many new things. I am really thankful to them.

Secondly, I would like to thank my father, my mother, my wife, my brothers, my sister and friends who helped me a lot in finalizing this thesis within the limited time frame.

Finally, I would like to dedicate my job to the spirit of my grandfather “Abdulhadi Hussein Jassim AL- TAMEEMI” and to my son “Ali”.

## NOMENCLATURE

$k$	thermal conductivity, W/m. K
$C$	specific heat, J/kg K
$k_b$	Boltzman constant, $1.381 \times 10^{-23}$ , J/K
$d_f$	base fluid molecular diameter, nm
$d_p$	nanoparticle diameter, nm
$f$	friction factor
$h$	heat transfer coefficient, W/m <sup>2</sup> . K
$Q$	total heat transfer rate, W
$q''$	wall heat flux, W/m <sup>2</sup>
$T$	temperature, K
$D_h$	hydraulic diameter, m
$L$	duct length, m
$Nu$	average Nusselt number, $hD_h / k_{nf}$
$p$	pressure, Pa
$Pe$	Peclet number, $U D/\alpha$
$Pr$	Prandtl number, $\nu/\alpha$
$Re$	Reynolds number, $U D_h / \nu$
$U$	Average velocity, m/s

### Subscripts

bf	base fluid
fr	freezing point
nf	nanofluid



p	nanoparticle
w	wall condition
in	inlet condition
out	outlet condition

### **Greek Letters**

$\psi$	sphericity
$\phi$	nanoparticle volumetric fraction in nanofluid
$\alpha$	thermal diffusivity, $\text{m}^2/\text{s}$
$\nu$	kinematic viscosity, $\text{m}^2/\text{s}$
$\rho$	density $\text{kg}/\text{m}^3$
$\mu$	viscosity $\text{N}\cdot\text{s}/\text{m}$

## TABLE OF CONTENTS

STATEMENT OF NON-PLAGIARISM.....	iii
ABSTRACT.....	iv
ÖZ.....	v
ACKNOWLEDGMENTS.....	vi
NOMENCLATURE.....	vii
TABLE OF CONTENTS.....	ix
LIST OF FIGURES.....	xii
LIST OF TABLES.....	xiv
INTRODUCTION AND LITRATURE REVIEW.....	1
1.1 Introduction.....	1
1.2 Literature Review.....	2
1.2.1 Nanoparticle Material and Base Liquid.....	2
1.2.2 Effects of Nanoparticle Volume Fraction.....	3
1.2.3 Effect of Nanoparticle Diameter.....	4
THERMOPHYSICAL PROPERTIES OF NANOFUIDS.....	6
2.1. Introduction.....	6
2.1.1 Density.....	7
2.1.2 Specific Heat Capacity.....	8
2.1.3 Thermal Conductivity.....	10
2.1.4 Viscosity.....	14

MATHEMATICAL FORMULATION OF THE PROBLEM .....	17
3.1 Introduction .....	17
3.1.1 Single Phase Model.....	17
3.1.2 Multi-Phase Model.....	18
3.2 Governing Equations .....	18
3.2.1 Reynolds Averaged Equations .....	18
3.2.2 Continuity Equation .....	20
3.2.3 Momentum (Navier-Stokes) Equations.....	22
3.2.4 Energy Equation.....	24
3.3 Turbulence Models .....	25
3-3-1 Realizable k- $\epsilon$ Model.....	26
3.4 Boundary Conditions.....	29
3.5 Calculation of Mixture Properties .....	30
3.5.1. Density Calculation.....	30
3.5.2 Specific Heat .....	31
3.5.3 Thermal Conductivity .....	31
3.5.4 Viscosity.....	32
3.6. Calculation of Nusselt Number .....	33
3.7. Calculation Friction Coefficient.....	34
NUMERICAL SOLUTION .....	36
4.1 ANSYS PROGRAM .....	36
4.2 Finite Volume Differencing Schemes .....	37
4.3 Numerical Simulation.....	41
4.3.1 Number of Iterations and Convergence .....	42
4.4 Grid Independence Analysis and Validation of Numerical Results.....	43

4.5 Validation Study for Nanofluids .....	46
RESULTS AND DISCUSSION .....	48
5.1 Geometry of Problem .....	48
5.2 The Effect of Nanoparticle Concentration on Heat Transfer .....	49
5.3 The Effect of Nanoparticle Diameter on the Heat Transfer .....	49
5.4 The Effect of Nano Particle Type on Nusselt Number.....	50
5.5 Variation of the Heat Transfer Coefficient.....	51
5.6 The Effect of Nanoparticles Type on Wall Shear Stress.....	52
5.7 The Effect of Volume Friction on Wall Shear Stress.....	53
CONCLUSION .....	54
6.1 Summary .....	54
6.2 Conclusions .....	55
6.3 Future Work .....	55
REFERENCES.....	57

## LIST OF FIGURES

<b>Figure 1</b> Turbulent velocity fluctuation as a function of time.....	19
<b>Figure 2</b> Geometry and coordinate system of the problem. ....	29
<b>Figure 3</b> The geometry for a single control volume in a two -dimensional Cartesian mesh .....	39
<b>Figure 4</b> Number of iterations and residual monitors. ....	43
<b>Figure 5</b> Geometry test for pure water .....	43
<b>Figure 6</b> Variation of Nusselt number with Reynolds number at different mesh densities for pure water , empirical correlation and Ajeel et al .(2017).....	45
<b>Figure 7</b> Grid distribution of square cross section duct. ....	45
<b>Figure 8</b> Comparison of friction coefficients obtained from Blasius formulation and present study. ....	46
<b>Figure 9</b> Comparison of the present result with results of Kaya et al .(2015) for nanofluids $Al_2O_3$ – water at $\phi=0.03$ .....	47
<b>Figure 10</b> Geometry study of the problem. ....	48
<b>Figure 11</b> Variation of Nusselt number with Reynolds number and volume fraction for $Al_2O_3$ - water mixture.....	49
<b>Figure 12</b> Variation of Nusselt number with Reynolds number at different nanoparticle diameters for $Al_2O_3$ -water mixture. ....	50
<b>Figure 13</b> Variation of Nusselt number with Reynolds number for different nanoparticles ( $Al_2O_3$ ,CuO and ZnO) - water mixtures at volume fraction 4% .....	51
<b>Figure 14</b> Variation of heat transfer coefficient with Reynolds number for pure water and $Al_2O_3$ - water mixture at volume fraction 4 % .....	52
<b>Figure 15</b> Variation of shear stress with Reynolds number for different nanofluids ( $Al_2O_3$ and CuO)- water mixture at volume fraction of 4%. ....	53

**Figure 16** Variation of shear stress along the channel for pure water and nonfluid Al<sub>2</sub>O<sub>3</sub> of volume fraction from 1-4% at Reynolds number of 35000.....53



## LIST OF TABLES

Table 1 Thermo-physical properties for water and $\text{Al}_2\text{O}_3$ , CuO and ZnO.....	30
Table 2 Correlations used for calculation of nanofluid properties.....	32
Table 3 Nanofluid thermo - physical properties with different volume fractions.....	33
Table 4 Finite volume differencing schemes. ....	41
Table 5 Friction factor for different Reynolds number. ....	46

## CHAPTER I

### INTRODUCTION AND LITRATURE REVIEW

#### 1.1 Introduction

Nanofluid is a new class of conventional heat transfer fluid that contains suspended nanoparticles that are less than 100 nm in size. Nanoparticles have a very significant effect in improving the heat transfer characteristics if they are mixed with a base fluid. It has been found that adding nanoparticles of specific materials such as metals oxides and carbon nanotubes to a base fluid such as water or oil, the thermal properties will improve and subsequently heat transfer would increase.

Despite the considerable attention to this new fluid in recent years, it is still under test in laboratories all over the world. Heat transfer characteristics of nanofluids have been investigated using experimental and numerical techniques.

In this study, nanofluid flow and heat transfer through a square cross-sectioned duct are analyzed. Water is used as the base fluid.  $\text{Al}_2\text{O}_3$ , CuO and ZnO particles are used as nano particles. It is considered that the flow is turbulent and a constant heat flux is applied over top and bottom walls. Because of the size and volume constraints, the square cross-sectioned flow-passages are commonly seen in compact heat exchangers. Non-circular ducts have lower heat exchange rate compared with a circular duct. Use of nanofluids in these systems might compensate the lower heat transfer rate.

Researcher's goal of studying these kinds of problems is to improve the thermal performance of heat exchangers involving square cross-sectioned flow passages. As the pressure drop also increases, the optimum design of such system requires good understanding of both the hydrodynamic and heat transfer characteristics of the problem.



In this thesis, using a numerical method, the effects of nano particle volume fraction, nano particle size, Reynolds number and material of the nano particles on the heat transfer rate (Nusselt number) and (friction coefficient) were investigated.

## **1.2 Literature Review**

In this section, studies found in the literature about nonofluids are summarized. The literature review is divided in three parts:

- Studies on nanoparticle and base liquid
- Nanoparticle volume concentration
- Nanoparticle diameter

### **1.2.1 Nanoparticle Material and Base Liquid**

The nanofluids can be categorized by nanoparticles and base fluids. Generally, nanoparticle materials are oxide ceramics ( $\text{Al}_2\text{O}_3$  and  $\text{CuO}$ ), metal carbides  $\text{SiC}$ , nitrides ( $\text{AlN}$ ,  $\text{SiN}$ ), metals ( $\text{Al}$  and  $\text{Cu}$ ) and non-metals (graphite and carbon nanotubes). Base fluids are water, ethylene, ethylene-glycols and oil.

Yarmand et al. (2014) carried out a numerical study about turbulent convection heat transfer in a rectangular channel. The continuity, momentum and energy equations were solved by using finite volume method for different types of nanoparticles ( $\text{Al}_2\text{O}_3$ ,  $\text{ZnO}$ ,  $\text{CuO}$  and  $\text{SiO}_2$ ) in the range of Reynolds number from 5000 to 25000. The volume fraction was between 1-5 %. The results indicated that the mixture of  $\text{SiO}_2$ - $\text{H}_2\text{O}$  nanofluid has Nusselt number bigger than the others nanofluids while it has lower heat transfer coefficient compared with the others nanofluids.

Ebrahimnia-Bajestan et al. (2011) investigated numerically the heat transfer performance and pressure drop using different nanoparticles ( $\text{Al}_2\text{O}_3$ ,  $\text{CuO}$ , carbon nanotube (CNT)) dispersed in water and ethylene glycol/water with particle concentrations of 0–6% through a straight circular pipe. The laminar flow regime was considered and a constant heat flux was applied. The results indicated that the heat transfer characteristics of

nanofluids are powerfully influenced by the type of base fluid.

Mohammad et al. (2011) studied heat transfer coefficient in laminar, steady state, three-dimension flow in a square shaped microchannel heat exchanger with four kinds of nanoparticles ( $\text{Al}_2\text{O}_3$ ,  $\text{SiO}_2$ , Ag and  $\text{TiO}_2$ ). The base fluid was water and different volume fractions (2%,5% and 10%) were considered. The results showed heat transfer coefficient increases by increasing Reynolds number. It was also found that the heat transfer coefficient in nanofluid  $\text{Al}_2\text{O}_3$ - $\text{H}_2\text{O}$  mixture is higher compared with pure water and others nanoparticles.

Hwang et al. (2006) showed in their study that nanofluids have higher thermal conductivity than that of base fluid. Through their study with four different types of nanofluids such as (MWCCTN, CuO,  $\text{SiO}_2$ ) in base fluid (water) and CuO in base fluid ethylene glycol, thermal conductivity was measured using transient hot-wire method. Thermal conductivity in nanofluid MWCCTN-water mixture at volume fraction 0.01 was increased up to 11.3%. Results show that thermal conductivity augmentation of nanofluids depends on the thermal conductivities of both particles and the base fluid.

### **1.2.2 Effects of Nanoparticle Volume Fraction**

Volume concentration (or volume fraction) can be accounted as one of the most important parameter of nanofluids. It is defined as the ratio of the volume of nanoparticles to the total volume (base fluid volume + nanoparticles volume). The solid particles have higher thermal conductivity than the liquid, therefore as the percentage of dispersed nanoparticles increases, the thermal conductivity of the whole mixture increases as well. For all of the considered volume fractions, the skin friction decreases by increasing the Reynolds number. while, the pressure drop increases by increasing volume fractions and Reynolds number.

Abdolbaqi et al. (2014) studied numerically turbulent flow in a straight square channel under constant heat flux with different kinds of solid nanoparticles (CuO,  $\text{TiO}_2$  and  $\text{Al}_2\text{O}_3$ ) suspended in base fluid (water). The mixture volume concentration ratio was varied

between 1-4%. They used CFD technique analysis by Fluent by using finite volume method and the top and bottom walls supplied with constant heat flux and uniform axial velocity at inlet. The results show that the heat transfer rates and wall shear stress increase by increasing volume concentration ratio.

Ting and Hou (2015) studied numerically laminar flow in square-sectioned duct under constant heat flux by using  $\text{Al}_2\text{O}_3$  nanoparticle with water. The effects of volume fraction on the heat transfer were investigated. The nanoparticle mixtures with the volume fractions 0.2, 0.5, 1.5, 2 and 2.5% were considered. It was found that the heat transfer coefficient of  $\text{Al}_2\text{O}_3$  at volume fraction 2.5 % was highest compared with the other mixtures.

Eastman et al. (1999) made a comparison between the thermal conductivity of nanofluid CuO-water mixture and pure water. They found that the thermal conductivity was approximately 20 percent higher when the concentration ratio is 5%. In addition, the optimization percentage for heat transfer coefficient was observed 15 percent compared with the base fluid when used 1% particles under the turbulent flow condition.

Wen and Ding (2004) studied nanofluid  $\text{Al}_2\text{O}_3$ /water heat transfer in laminar flow under constant wall heat flux and reported an increase in nanofluid heat transfer coefficient with Reynolds number and nanoparticles concentration particularly at the entrance region. They observed that the thermally developing length for nanofluid was greater than pure water.

### **1.2.3 Effect of Nanoparticle Diameter**

Nanoparticle diameter is another effective parameter which has an important role in the hydraulic and thermal behaviors of nanofluids. Mirmasoumi and Behzadmehr (2008) investigated numerically the effects of nanoparticle diameter on the heat transfer for  $\text{Al}_2\text{O}_3$ -water flow under a fully developed laminar flow regime. It was explored that by decreasing the nanoparticle diameter, markedly increased the heat transfer coefficient value of the nanofluid. However, the nanoparticle diameter did not have much effect on

the skin friction coefficient.

Heris et al. (2066, 2007) studied experimentally and numerically the heat transfer coefficient for different type of nanoparticles  $\text{Al}_2\text{O}_3$  and  $\text{CuO}$  mixture in pure water. They investigated the heat transfer coefficient for nanofluid ( $\text{Al}_2\text{O}_3$ -water). The conditions were laminar flow in a circular tube, at inlet of the tube the velocity and temperature were taken as uniform, the outlet pressure is fixed and the wall temperature is fixed. They reported when nanoparticle diameter decreases, the heat transfer coefficient increases.

Namburu et al. (2009) studied turbulent nanofluid flows for three different nanoparticles ( $\text{CuO}$ ,  $\text{Al}_2\text{O}_3$  and  $\text{SiO}_2$ ) in different base fluids (ethylene glycol, water) through a circular tube supplied with constant heat flux. Results showed that the smaller nanoparticle diameters cause high mixture viscosity.

Minakof et al. (2016) experimentally investigated turbulent forced convection heat transfer in a cylindrical channel by using nanoparticles  $\text{SiO}_2$  and  $\text{Al}_2\text{O}_3$  with mixture ratios between 0.5 and 2%. The nanoparticle size was changed from 10 to 100 nm. The pressure drop and heat transfer coefficient from the concentration, size, temperature and kind of nanoparticles material were studied. It was shown that nanoparticles added to the coolant have meaningfully effects in the heat transfer coefficient in the turbulent flow regime. It is shown that the local heat transfer coefficient at a fixed value of Reynolds number was increased by increasing nanoparticles concentration.

## CHAPTER II

### THERMOPHYSICAL PROPERTIES OF NANOFLUIDS

#### 2.1. Introduction

The concept behind development of nanofluids is to use them as thermal fluids in heat exchangers for augmentation of heat transfer coefficient and minimize the size of heat transfer equipment. The properties (density, specific heat, thermal conductivity and viscosity) are parameters which influence the heat transfer characteristics of nanofluids. Operating temperature has important effects to thermo physical properties. Determination of the thermo physical properties of nanofluids is necessary for the analysis of nanofluid flow and heat transfer.

Xuan and Roetzel (2000) showed that the transport properties of nanofluids change when nano particles are added to a base fluid because the particles exhibit a great potential in enhancing heat transfer based on the hypothesis that the nanofluid performs more like a fluid rather than a conventional solid–fluid mixture.

In studies found in the literature, the nanofluid properties are often compared with base fluid properties in nanofluid heat transfer research. The relative properties are given bellow:

$$k_r = \frac{k_{nf}}{k_{bf}} \quad (2.1)$$

$$\mu_r = \frac{\mu_{nf}}{\mu_{bf}} \quad (2.2)$$

$$\rho_r = \frac{\rho_{nf}}{\rho_{bf}} \quad (2.3)$$

$$C_r = \frac{C_{nf}}{C_{bf}} \quad (2.4)$$

In Equations (2.1- 2.4),  $\mu$  ,  $\rho$ ,  $C$  and  $k$  are viscosity, density, specific heat and thermal conductivity, respectively. Subscript  $r$  refers to relative,  $nf$  refers to nanofluid and  $bf$  refers to base fluid properties.

### 2.1.1 Density

The effective density of the nanofluid can be estimated based on the physical principle of the mixtures as given in the following equations Wang et al. (2008).

$$\rho_{nf} = \frac{m_T}{V_T}$$

$$\rho_{nf} = \frac{m_{bf} + m_p}{V_{bf} + V_p}$$

$$\rho_{nf} = \frac{\rho_{bf}V_{bf} + \rho_p V_p}{V_{bf} + V_p}$$

The above equation can be written as:

$$\rho_{nf} = \frac{V_{bf} + V_p - V_p}{V_{bf} + V_p} \rho_{bf} + \frac{V_p}{V_{bf} + V_p} \rho_p$$

Noting that

$$\phi = \frac{V_p}{V_{bf} + V_p}$$

$$\rho_{nf} = (1 - \phi)\rho_{bf} + \phi\rho_p \quad (2.5)$$

From the analysis of Eq. (2.5) we can make the following observations about the density of a nanofluid:

- Mixture density is bigger than that of the base liquid.
- As the particle volume fraction increases, the nanofluid density increases.

### 2.1.2 Specific Heat Capacity

In general, most of the literatures indicate that the specific heat capacity can be calculate from two different models which are widely used in the nanofluid literature.

#### Model I

For this model, a mixing theory similar to the theory for ideal gas mixtures is considered (Zhou et al.; 2008). It is a weighted average of the base fluid specific heat,  $C_{bf}$  and nanoparticle specific heat,  $C_p$ . Based on this model, the nanofluid specific heat can be expressed as,

$$C_{nf} = \phi C_p + (1 - \phi)C_{bf} \quad (2.6)$$

Although this is simple, it is commonly used.

#### Model II

Buongiorno et al. (2006) and Zhou et al. (2008) suggested a model based on the assumption of thermal equilibrium between the nano particles and the surrounding fluid. For an arbitrary mass and volume of nanofluid with a nanoparticle volume fraction, we can write,

$$(\rho C)_{nf} = \rho_{nf} \left( \frac{Q}{m \Delta T} \right)_{nf}$$

$$(\rho C)_{nf} = \rho_{nf} \frac{Q_{bf} + Q_p}{(m_{bf} + m_p) \Delta T}$$

$$(\rho C)_{nf} = \rho_{nf} \frac{(m C_p)_{bf} \Delta T + (m C_p)_p \Delta T}{(m_{bf} + m_p) \Delta T}$$

$$(\rho C)_{nf} = \rho_{nf} \frac{(\rho C_p)_{bf} V_{bf} + (\rho C_p)_p V_p}{\rho_{bf} V_{bf} + \rho_p V_p}$$

Noting that:

$$\rho_{nf} = \frac{m_{nf}}{V_{nf}}$$

$$m_{nf} = \rho_{bf} V_{bf} + \rho_p V_p$$

$$\phi = \frac{V_p}{V_{bf} + V_p}$$

Where

$m_{nf}$  is total mass of nanofluid.

$V_{nf}$  is total volume of nanofluid.

$\rho_{bf}$  is density of base fluid.

$\rho_p$  is density of nano particle.

$V_{bf}$  is volume of base fluid.

$V_p$  is volume of nano particle.

$$(\rho C)_{nf} = (1 - \phi_p)(\rho C_p)_{bf} + \phi_p (\rho C_p)_p$$



Finally, this formula can be rewritten as:

$$C_{nf} = \frac{(1-\phi)(\rho C)_{bf} + \phi(\rho C)_p}{\rho_{nf}} \quad (2.7)$$

Where  $C_p$  and  $C_{bf}$  are the heat capacities of the nanoparticles and the base fluid, respectively.

O'Hanley et al. (2012) showed that these two models give considerably different results for a given nanofluid. Comparison with the experimental results shows that Model II is in a good agreement, whereas, the predictions of Model I differs from the experimental data.

From the analysis of Eq. (2.7) we can make the following observations:

- The specific heat value of nanofluid is lower compared to the base liquid.
- Increasing concentration in mixture makes specific heat to decrease.
- The temperature does not have a significant impact on specific heat of nanofluid.
- The material of nano particle and nanoparticle diameter do not have effect on specific heat of nanofluid because the specific heat for base fluid is very high compared with nanoparticles. The variation of heat capacity with volume concentration is small.

### **2.1.3 Thermal Conductivity**

There is no dependable theory to estimate the thermal conductivity of nano fluids (Wang et al, 2008). From experimental studies of many researchers, it is known that the thermal conductivity of nanofluids depends on the thermal conductivities of the base fluid and the nanoparticles, the volume fraction, the surface area and the shape of the nanoparticles, and the temperature. There are no theoretical formulas currently available to predict the thermal conductivity of nanofluids satisfactorily.

For the theoretical studies, specific heat of the nano particle mixtures have been based on the classical work of Maxwell et al. (1881). The Maxwell model is perfect for solid particle

and liquid mixtures at low concentrations. Based on this, the thermal conductivity for nano particles mixture is given by:

$$k_{nf} = \frac{k_p + 2k_{bf} + 2(k_p - k_{bf})\phi}{k_p + 2k_{bf} - 2(k_p - k_{bf})\phi} k_{bf} \quad (2.8)$$

where

$k_p$  is the thermal conductivity for nano particle.

$k_{bf}$  is the thermal conductivity for base fluid.

$\phi$  is the volume fraction (concentration).

Maxwell's formula is the effective thermal conductivity of mixture which is depended on the thermal conductivity of the spherical particle, base fluid and the concentration.

Bruggeman et al. (1935) offered a model to evaluate the interactions between randomly dispersed particles. For a binary mixture of homogeneous spherical inclusions, the Bruggeman model gives following equation:

$$\phi \left( \frac{k_p + k_{nf}}{k_p + 2k_{nf}} \right) + (1 - \phi) \left( \frac{k_{bf} - k_{nf}}{k_{bf} + 2k_{nf}} \right) = 0 \quad (2.9)$$

This model can be used without restrictions for spherical particles on the concentration of inclusions. The results for the Bruggeman model and the Maxwell model generally are the same and they have high sufficiently when used in law solid particle concentration. The Maxwell model in experimental results fails to offer a good match. But, the Bruggeman model gives a good agreement with the experimental data.

Choi et al. (1995) and Hamilton et al. (1962) proposed a model for liquid-solid mixtures of non-spherical particles. They inserted a shape factor,  $n$ , to compute the effect of the shape of the particles. The thermal conductivity ratio between the solid and fluid phases conductivity is greater than 100 ( $k_p / k_{nf} > 100$ ), the thermal conductivity of nanofluids can be written as follows:

$$k_{nf} = \frac{k_p + (n-1)k_{bf} - 2(n-1)(k_{bf} - k_p)}{k_p + (n-1)k_{bf} + (k_p - k_{bf})\phi} k_{bf} \quad (2.10)$$

where  $n$  is the empirical shape factor given by  $n = 3/\psi$ ,  $\psi$  is the particle sphericity and it is the ratio between the surface area of a sphere (with the same volume as the given particle) to the surface area of the particle.

Yu and Choi (2003) modified the Maxwell model and proposed the following model:

$$k_{pe} = \frac{[2(1-\gamma) + (1+\beta)^3(1+2\gamma)\gamma]}{-(1-\gamma) + (1+\beta)^3(1+2\gamma)} k_p \quad (2.11)$$

where layer  $\gamma = k_{layer} / k_p$  is the ratio of nano-layer thermal conductivity to particle thermal conductivity and  $\beta = h / r$  is the ratio of the Nano-layer thickness to the original particle radius. Hence, the Maxwell equation (Eq. (2.8)) can be re-cast as follows

$$k_{nf} = \frac{k_p + 2k_{bf} + 2(k_p - k_{bf})(1+\gamma)^3\phi}{k_p + 2k_{bf} - 2(k_p - k_{bf})(1+\gamma)^3\phi} k_{bf} \quad (2.12)$$

Corcione et al. (2011) proposed an empirical correlation based on many of experimental data available in the literature to calculate thermal conductivity of nanofluid and this empirical correlation is valid to use for nanoparticle diameter ranging from 10 to 150 nm and volume fraction from 0.002 to 0.09, while, the temperature ranging from 294 K to 324 K. Mean deviation of this correlation is 1.86 %.

$$\frac{k_{nf}}{k_{bf}} = 1 + 4.4\text{Re}^{0.4}\text{Pr}^{0.66} \left(\frac{T}{T_{fr}}\right)^{10} * \left(\frac{k_p}{k_{bf}}\right)^{0.03} * \phi^{0.66} \quad (2.13)$$

Where Re is the Reynolds number for nanoparticle, Pr is the Prandtl number of the base fluid, T is the temperature,  $T_{fr}$  is the freezing point of the base liquid,  $k_p$  is the thermal conductivity for nanoparticle, and  $\phi$  is the volume fraction of the suspended nanoparticles.

$$\text{Re} = \frac{\rho_{bf} u_B d_p}{\mu_{bf}} \quad (2.14)$$

Where  $d_p$  is the nanoparticle diameter and  $u_b$  is the mean Brownian velocity and it is the ratio between  $d_p$  and time required  $\tau_D$  to cover such distance according to Koblinski et al. (2002).

$$\tau_D = \frac{d_p^2}{6D} = \frac{\pi\mu_{bf}d_p^3}{2k_bT} \quad (2.15)$$

where  $D$  is the Einstein diffusion coefficient and  $k_b$  is the Boltzmann's constant. Hence

$$u_B = \frac{2k_bT}{\pi\mu_{bf}d_p^2} \quad (2.16)$$

Substituting Eq. (2.16) into (2.14) then

$$\text{Re} = \frac{2\rho_{bf}k_pT}{\pi\mu_{bf}^2d_p} \quad (2.17)$$

From the above, we can make the following observations for the thermal conductivity of nanofluids:

- The metals and oxides nanoparticles are observed have higher thermal conductivity than base fluids.
- Generally, the nanoparticle diameter is taken from experimental data to find thermal conductivity were (20-300 nm) and temperatures range were between (20 - 70 °C) at maximum volume concentration 4.0% in base liquids (water, EG, and EG/water).
- Most experimental results have set the thermal conductivity of nano particles is higher than base fluid, also the result shows that the thermal conductivity increases by increasing concentration.
- Thermal conductivity in the most literatures indicate that an ethylene glycol-based nanofluids is a higher than that pure water-based nanofluids.

- Metal nanoparticles is the better than of oxide nanoparticles for enhancing heat transfer.
- Nanoparticle diameter and temperature have big effect on thermal conductivity.
- Thermal conductivity of nanofluid is dependent on material properties.

#### 2.1.4 Viscosity

Viscosity is a significant flow property of fluids. Viscosity plays important roles on pumping power, pressure drop and heat transfer. In recent years, different correlations are proposed for nanofluid viscosity (Mahbubul et al., 2012). The first expression for nanofluid viscosity was proposed by Einstein (1906). His model is based on the assumption that the particle concentration is very low. It was expressed as,

$$\frac{\mu_{nf}}{\mu_{bf}} = 1 + 2.5\phi \quad (2.18)$$

Where

$\mu_{bf}$  is the viscosity of base fluid.

$\mu_{nf}$  is the viscosity of the nanofluid

Equation (2.18) is valid in the range of volume fraction from 0 to 0.02. As seen in this equation, the viscosity of the nanofluid increases linearly with the volume fraction. Krieger et al. (1959) proposed a semi empirical model for nanofluid viscosity for full range of particle volume fraction. The model is given below:

$$\frac{\mu_{nf}}{\mu_{bf}} = \left[ 1 - \frac{\phi}{\phi m} \right]^{-\eta\phi} \quad (2.19)$$

Where

$\phi m$  is the maximum particle packing fraction.

$\eta$  is the intrinsic viscosity. For monodispersed sphere suspensions, its value is 2.5.

Nielsen (1970) proposed the power law model to calculate the viscosity of nanofluids. His model is good for mixtures with volume fraction more than 0.02 and it is as follows:

$$\mu_{nf} = (1 + 1.5\phi) \exp^{\frac{\phi}{1-\phi^m}} \mu_f \quad (2.20)$$

Modifying the Einstein viscosity equation, Batchelor (1977) developed following model for isotropic suspension of spherical nanoparticles.

$$\mu_{nf} = (1 + 2.5\phi + 6.5\phi^2) \mu_{bf} \quad (2.21)$$

Equation (2.18) – Eq. (2.21), in this survey are classical models to calculate the viscosity for nanofluids. With research on the study on viscosity of nanoparticles, there are lots of different models which are developed by modifying these classical models.

Brinkman (1952) suggested a model similar to the Einstein's model for particle volume concentration less than 4%. The expression suggested by Brinkman is as follows:

$$\mu_{nf} = \frac{\mu_{bf}}{(1-\phi)^{2.5}} \quad (2.22)$$

Corcione et al. (2011) proposed an empirical correlation based on many experimental data available in the literature to calculate viscosity of nanofluid. This empirical correlation is valid for nanoparticles of diameter ranging from 25 to 200 nm and volume fraction from 0.0001 to 0.071%, while, the temperature ranging from 293 K to 323 K.

$$\frac{\mu_{nf}}{\mu_{bf}} = \frac{1}{1 - 34.87 \left( \frac{d_p}{d_f} \right)^{-0.03} \phi^{1.03}} \quad (2.23)$$

$d_f$  is an equivalent diameter of base fluid, which is calculated as,

$$d_f = 0.1 \left( \frac{6M}{N \pi \rho_{bf}} \right)^{\frac{1}{3}} \quad (2.24)$$

M is the molecular weight of the base fluid; N is the Avogadro number,

From the analysis we can make the following observations about the viscosity of a nanofluid:

- Nanofluid viscosity increases by increasing concentration.
- Nanofluid viscosity decreases by increasing the temperature.
- Nanofluid viscosity increases by decreasing nanoparticle size.
- The nature of the material does not significantly affect the viscosity of nanofluid.



## CHAPTER III

### MATHEMATICAL FORMULATION OF THE PROBLEM

#### 3.1 Introduction

In this study, a duct with square cross-section is considered. A nanofluid flows through the channel. The base fluid is considered to be water. Nano particles considered are  $\text{Al}_2\text{O}_3$ ,  $\text{CuO}$  and  $\text{ZnO}$ . The nanoparticles and the base fluid are flowing in the same domain. Hence, in true sense the flow is a two-phase flow. In the literature, there are studies modelling the nanofluid flow as single phase and also as multi-phase flows.

##### 3.1.1 Single Phase Model

In most nanofluid flows, particle size is very small hence, it can be assumed that particles move with the same velocity as the base fluid, and particles and base fluid are in local thermal equilibrium. Under such conditions, single phase flow model can be used. In single flow modelling, the fluid properties are calculated considering nano particle volume fraction in the mixture using the correlations proposed in the literature. Then a single set of equations are solved in whole flow field.

In this study, it is assumed that local velocity of both phases are the same and the phases are in local thermal equilibrium, hence single phase flow model is used. In this model it is also assumed that the nano particle volume fraction is homogeneous over the whole flow domain. The other flow properties such as density, thermal conductivity, specific heat and viscosity are calculated using expressions developed for homogeneous mixtures. These correlations were given in Chapter 2.



### **3.1.2 Multi-Phase Model**

Truly speaking, nanoparticle-fluid mixtures are multi-phase. In some cases, the particle and the fluid velocities and temperature may differ locally in the flow field. For the analysis of such cases, the theory of the classical multi-phase flow has been applied for nanoparticle mixtures. In this model the nanoparticles and the base fluid are considered as two different phases with different velocities and temperatures. In multi-phase flow model, the energy and momentum equations are solved for both phases separately in the same domain. The effects one phase on the other are accounted as sources in the governing equations.

## **3.2 Governing Equations**

The flow in the problem considered is steady, turbulent and three-dimensional forced convection flow. For the analysis of flow and heat transfer characteristics, the continuity, momentum and energy equations should be solved. Since the flow is turbulent, Reynolds averaged equations are considered and the turbulence is modelled using realizable  $k$ - $\varepsilon$  turbulence model.

### **3.2.1 Reynolds Averaged Equations**

In turbulent flows, the momentary value of a flow variable is decomposed into the mean value and fluctuating value. This is shown in Figure 1 for velocity component  $u$ .

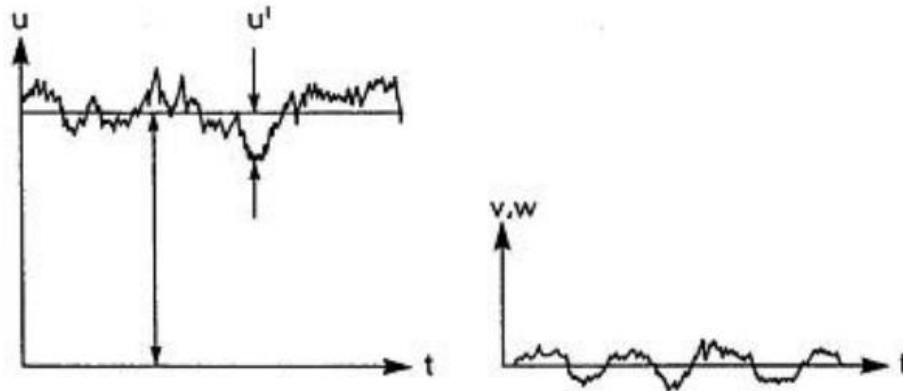


**Figure 1** Turbulent velocity fluctuation as a function of time.

The momentary value of a general variable  $f$  can be written as the sum of the time-averaged value  $\bar{f}$  and the fluctuating component  $f'$ .

$$f = \bar{f} + f' \quad (3.1)$$

The Reynolds averaging method takes the mean values at a fix point in space and average it over a time span that is large enough for the mean values to be independent of it. The time averaged value of any variable mathematically defined as

$$\bar{f} = \frac{1}{\Delta t} \int_{t_0}^{t_0 + \Delta t} f dt \quad (3.2)$$

Then the below time averaged expressions can be derived (Ghiaasiaan, 2011).

$$\overline{\bar{f}} = \bar{f} \quad (3.3)$$

$$\overline{f + g} = \bar{f} + \bar{g} \quad (3.4)$$

$$\overline{f \cdot g} = \bar{f} \cdot \bar{g} \quad (3.5)$$

$$\overline{\frac{\partial f}{\partial s}} = \frac{\partial \bar{f}}{\partial s} \quad (3.6)$$

$$\overline{\int f ds} = \int \bar{f} ds \quad (3.7)$$

$$\overline{f \cdot g} \neq \bar{f} \cdot \bar{g} \quad (3.8)$$

The time-averaged values of the fluctuating components are obtained to be zero, i.e.

$$\bar{f}' = 0$$

Similarly, the instantaneous velocity components, pressure, temperature and density of a turbulent flow can be expressed as below:

$$u = \bar{u} + u'$$

$$v = \bar{v} + v'$$

$$w = \bar{w} + w' \quad (3.9)$$

$$p = \bar{p} + p'$$

$$T = \bar{T} + T'$$

The time-averaged values of the fluctuating components are zero, i.e.

$$\bar{u}' = 0$$

$$\bar{v}' = 0$$

$$\bar{w}' = 0$$

$$\bar{p}' = 0$$

(3.10)

### 3.2.2 Continuity Equation

For an incompressible flow, the continuity equation in terms of instantaneous velocity components for an incompressible flow can be written as,

$$\frac{\partial u}{\partial x} + \frac{\partial v}{\partial y} + \frac{\partial w}{\partial z} = 0 \quad (3.11)$$

To obtain the time averaged continuity equation, we substitute the expressions for the velocities from Eq. (3.9), into above equation and then take the time average of the equation using the above given principles.

$$\frac{\partial \bar{u}}{\partial x} + \frac{\partial \bar{u}'}{\partial x} + \frac{\partial \bar{v}}{\partial y} + \frac{\partial \bar{v}'}{\partial y} + \frac{\partial \bar{w}}{\partial z} + \frac{\partial \bar{w}'}{\partial z} = 0 \quad (3.12)$$

By taking the time-average of the above equation, we get

$$\overline{\frac{\partial \bar{u}}{\partial x} + \frac{\partial \bar{u}'}{\partial x} + \frac{\partial \bar{v}}{\partial y} + \frac{\partial \bar{v}'}{\partial y} + \frac{\partial \bar{w}}{\partial z} + \frac{\partial \bar{w}'}{\partial z}} = 0 \quad (3.13)$$

Before reduction Eq. (3.13), bellow is summary of rules for time averaging.

$$\overline{\frac{\partial \bar{u}}{\partial x}} = \frac{1}{\Delta t} \int_{t_0}^{t_0+\Delta t} \frac{\partial u}{\partial x} dt \quad (3.14)$$

$$\overline{\frac{\partial \bar{u}}{\partial x}} = \frac{\partial}{\partial x} \frac{1}{\Delta t} \int_{t_0}^{t_0+\Delta t} u dt \quad (3.15)$$

$$\overline{\frac{\partial \bar{u}}{\partial x}} = \frac{\partial \bar{u}}{\partial x} \quad (3.16)$$

$$\overline{\frac{\partial \bar{u}'}{\partial x}} = \frac{1}{\Delta t} \int_{t_0}^{t_0+\Delta t} \frac{\partial u'}{\partial x} dt \quad (3.17)$$

$$\overline{\frac{\partial \bar{u}'}{\partial x}} = \frac{\partial}{\partial x} \frac{1}{\Delta t} \int_{t_0}^{t_0+\Delta t} u' dt \quad (3.18)$$

$$\overline{\frac{\partial \bar{u}'}{\partial x}} = 0 \quad (3.19)$$

The averaged derivatives of the fluctuations are also zero according to Eq. (3.19).

Using the above expressions, the continuity equation is reduced to

$$\frac{\partial \bar{u}}{\partial x} + \frac{\partial \bar{v}}{\partial y} + \frac{\partial \bar{w}}{\partial z} = 0 \quad (3.20)$$

$$\text{div}(\bar{V}) = 0 \quad (3.21)$$

### 3.2.3 Momentum (Navier-Stokes) Equations

For an incompressible flow, x-direction momentum equation in terms of instantaneous variables can be written as (neglecting body force):

$$\frac{\partial u}{\partial t} + u \frac{\partial u}{\partial x} + v \frac{\partial u}{\partial y} + w \frac{\partial u}{\partial z} = -\frac{1}{\rho} \frac{\partial p}{\partial x} + \nu \left( \frac{\partial^2 u}{\partial x^2} + \frac{\partial^2 u}{\partial y^2} + \frac{\partial^2 u}{\partial z^2} \right) \quad (3.22)$$

Multiplying the continuity equation by u and adding it to the above equation, we get,

$$u \left( \frac{\partial u}{\partial x} + \frac{\partial v}{\partial y} + \frac{\partial w}{\partial z} \right) = 0$$

$$\frac{\partial u^2}{\partial x} + \frac{\partial(uv)}{\partial y} + \frac{\partial(uw)}{\partial z} = -\frac{1}{\rho} \frac{\partial p}{\partial x} + \nu \left( \frac{\partial^2 u}{\partial x^2} + \frac{\partial^2 u}{\partial y^2} + \frac{\partial^2 u}{\partial z^2} \right) \quad (3.23)$$

To obtain the time averaged equation, we substitute the expressions for the instantaneous velocities from Eq. (3.9) into above equation and then take the time average of the equation using the above given principles. This averaging procedure yields the following equation:

$$\overline{\frac{\partial u^2}{\partial x}} + \overline{\frac{\partial(uv)}{\partial y}} + \overline{\frac{\partial(uw)}{\partial z}} = -\frac{1}{\rho} \overline{\frac{\partial p}{\partial x}} + \nu \left( \overline{\frac{\partial^2 u}{\partial x^2}} + \overline{\frac{\partial^2 u}{\partial y^2}} + \overline{\frac{\partial^2 u}{\partial z^2}} \right) \quad (3.24)$$

Substituting Eq. (3.9) to the above equation,

$$\left[ \frac{\partial(\bar{u})^2}{\partial x} + \frac{\partial(\overline{u'^2})}{\partial x} \right] + \left[ \frac{\partial(\bar{u}\bar{v})}{\partial y} + \frac{\partial(\overline{u'v'})}{\partial y} \right] + \left[ \frac{\partial(\bar{u}\bar{w})}{\partial z} + \frac{\partial(\overline{u'w'})}{\partial z} \right] = -\frac{1}{\rho} \frac{\partial \bar{p}}{\partial x} + \nu \left( \frac{\partial^2 \bar{u}}{\partial x^2} + \frac{\partial^2 \bar{u}}{\partial y^2} + \frac{\partial^2 \bar{u}}{\partial z^2} \right) \quad (3.25)$$

Where

$$\frac{\partial(\bar{u})^2}{\partial x} = 2\bar{u} \frac{\partial \bar{u}}{\partial x} \quad (3.26)$$

$$\frac{\partial(\bar{u}\bar{v})}{\partial y} = \bar{u} \frac{\partial \bar{v}}{\partial y} + \bar{v} \frac{\partial \bar{u}}{\partial y} \quad (3.27)$$

$$\frac{\partial(\bar{u}\bar{w})}{\partial z} = \bar{u} \frac{\partial \bar{w}}{\partial z} + \bar{w} \frac{\partial \bar{u}}{\partial z} \quad (3.28)$$

Substituting back

$$\left[ 2\bar{u} \frac{\partial \bar{u}}{\partial x} + \frac{\partial(\overline{u'^2})}{\partial x} \right] + \left[ \bar{u} \frac{\partial \bar{v}}{\partial y} + \bar{v} \frac{\partial \bar{u}}{\partial y} + \frac{\partial(\overline{u'v'})}{\partial y} \right] + \left[ \bar{u} \frac{\partial \bar{w}}{\partial z} + \bar{w} \frac{\partial \bar{u}}{\partial z} + \frac{\partial(\overline{u'w'})}{\partial z} \right] = -\frac{1}{\rho} \frac{\partial \bar{p}}{\partial x} + \nu \left( \frac{\partial^2 \bar{u}}{\partial x^2} + \frac{\partial^2 \bar{u}}{\partial y^2} + \frac{\partial^2 \bar{u}}{\partial z^2} \right) \quad (3.29)$$

Multiplying the time-averaged continuity equation by  $\bar{u}$

$$\bar{u} \left( \frac{\partial \bar{u}}{\partial x} + \frac{\partial \bar{v}}{\partial y} + \frac{\partial \bar{w}}{\partial z} \right) = 0 \quad (3.30)$$

Subtracting equation (3.29) with this equation, it yields

$$\left[ \bar{u} \frac{\partial \bar{u}}{\partial x} + \frac{\partial (\overline{u'^2})}{\partial x} \right] + \left[ \bar{v} \frac{\partial \bar{u}}{\partial y} + \frac{\partial (\overline{u'v'})}{\partial y} \right] + \left[ \bar{w} \frac{\partial \bar{u}}{\partial z} + \frac{\partial (\overline{u'w'})}{\partial z} \right] = -\frac{1}{\rho} \frac{\partial \bar{p}}{\partial x} + \nu \left( \frac{\partial^2 \bar{u}}{\partial x^2} + \frac{\partial^2 \bar{u}}{\partial y^2} + \frac{\partial^2 \bar{u}}{\partial z^2} \right) \quad (3.31)$$

After arrangement,

$$\bar{u} \frac{\partial \bar{u}}{\partial x} + \bar{v} \frac{\partial \bar{u}}{\partial y} + \bar{w} \frac{\partial \bar{u}}{\partial z} + \frac{1}{\rho} \frac{\partial \bar{p}}{\partial x} = \nu (\nabla^2 \bar{u}) - \frac{\partial (\overline{u'^2})}{\partial x} - \frac{\partial (\overline{u'v'})}{\partial y} - \frac{\partial (\overline{u'w'})}{\partial z} \quad (3.32)$$

$$\text{Where } \nabla^2 \bar{u} = \frac{\partial^2 \bar{u}}{\partial x^2} + \frac{\partial^2 \bar{u}}{\partial y^2} + \frac{\partial^2 \bar{u}}{\partial z^2} \quad (3.33)$$

Similar equations can be derived for y- and z-directions, and the resulting equations can be written in tensor notation as

$$\bar{u}_j \frac{\partial u_i}{\partial x_j} + \frac{1}{\rho} \frac{\partial \bar{p}}{\partial x} = \nu \left( \frac{\partial^2 \bar{u}_i}{\partial x_j \partial x_j} \right) - \left( \frac{\partial (\overline{u'_i v'_j})}{\partial x_j} \right) \quad (3.34)$$

In the above equation, the last three terms on the right hand side are known as the Reynolds stress terms. These terms represent the transported quantities for instance momentum, energy and species concentration resulting from the fluctuations in velocities, temperature, pressure, etc. These fluctuations are small scale, high frequency, and hence they are computationally exclusive to simulate directly in practical engineering calculations.

### 3.2.4 Energy Equation

Energy equation (neglect dissipation term):

$$\rho c_p \left( u \frac{\partial T}{\partial x} + v \frac{\partial T}{\partial y} + w \frac{\partial T}{\partial z} \right) = k \left( \frac{\partial^2 T}{\partial x^2} + \frac{\partial^2 T}{\partial y^2} + \frac{\partial^2 T}{\partial z^2} \right) \quad (3.35)$$

Multiplying continuity equation by T:

$$T \left( \frac{\partial u}{\partial x} + \frac{\partial v}{\partial y} + \frac{\partial w}{\partial z} \right) = 0 \quad (3.36)$$

Adding Eq. (3.36) to Eq. (3.35)

$$\left( \frac{\partial(uT)}{\partial x} + \frac{\partial(vT)}{\partial y} + \frac{\partial(wT)}{\partial z} \right) = \alpha \left( \frac{\partial^2 T}{\partial x^2} + \frac{\partial^2 T}{\partial y^2} + \frac{\partial^2 T}{\partial z^2} \right) \quad (3.37)$$

Averaging over period  $0 \rightarrow t_1$

$$\left( \overline{\frac{\partial(uT)}{\partial x}} + \overline{\frac{\partial(vT)}{\partial y}} + \overline{\frac{\partial(wT)}{\partial z}} \right) = \alpha \left( \overline{\frac{\partial^2 T}{\partial x^2}} + \overline{\frac{\partial^2 T}{\partial y^2}} + \overline{\frac{\partial^2 T}{\partial z^2}} \right) \quad (3.38)$$

$$\text{After arrangement, } \left( \overline{\frac{\partial(uT)}{\partial x}} + \overline{\frac{\partial(vT)}{\partial y}} + \overline{\frac{\partial(wT)}{\partial z}} \right) = \alpha \left( \overline{\frac{\partial^2 T}{\partial x^2}} + \overline{\frac{\partial^2 T}{\partial y^2}} + \overline{\frac{\partial^2 T}{\partial z^2}} \right) \quad (3.39)$$

$$\begin{aligned} & \left[ \bar{u} \frac{\partial \bar{T}}{\partial x} + \bar{T} \frac{\partial \bar{u}}{\partial x} \right] + \left[ \bar{v} \frac{\partial \bar{T}}{\partial y} + \bar{T} \frac{\partial \bar{v}}{\partial y} \right] + \left[ \bar{w} \frac{\partial \bar{T}}{\partial z} + \bar{T} \frac{\partial \bar{w}}{\partial z} \right] + \frac{\partial(\overline{uT'})}{\partial x} + \frac{\partial(\overline{vT'})}{\partial y} + \frac{\partial(\overline{wT'})}{\partial z} = \\ & \alpha \left( \overline{\frac{\partial^2 T}{\partial x^2}} + \overline{\frac{\partial^2 T}{\partial y^2}} + \overline{\frac{\partial^2 T}{\partial z^2}} \right) \end{aligned} \quad (3.40)$$

$$\text{div}(\rho \bar{V} C_p \bar{T}) = \text{div}(k \nabla \bar{T} - \rho C_p \bar{u}' T') \quad (3.41)$$

### 3.3 Turbulence Models

Turbulent flows are categorized by fluctuating pressure, velocity and temperature fields. These fluctuations result in fluctuation of transported quantities for instance momentum, energy and species concentration. These fluctuations are small scale, high frequency, and they are also computationally exclusive to simulate directly in practical engineering calculations.



The governing equations were defined in section (3-2) are normally time-averaged to eliminate the small scales. The resulting reformed set of equations is computationally less expensive to solve the modified equations comprise unknown variables, and turbulence models are required to determine these variables in expressions of known quantities. Generally, there are many choices of turbulence models as,

- Spalart-Allmaras model
- k-ε models
- k-ω models
- Reynolds stress model (RSM)
- Large eddy simulation (LES) model

In this study realizable k-ε model is used. This model is formulated below.

### **3-3-1 Realizable k- ε Model**

The realizable k-ε model is different from the standard k-ε model in two main ways:

- (a) The realizable k-ε model comprises an alternate turbulent viscosity formulation.
- (b) A modified transport equation for the dissipation rate, ε, has been derived from an exact equation for the transport of the mean square vorticity fluctuation.

The transport equations for turbulent kinetic energy, k and turbulent kinetic energy dissipation, ε in the realizable k-ε model are as given below (Shih et al, 1995):

$$\frac{\partial}{\partial t}(\rho k) + \frac{\partial}{\partial x_j}(\rho k u_j) = \frac{\partial}{\partial x_j} \left[ \left( \mu + \frac{\mu_t}{\sigma_k} \right) \frac{\partial k}{\partial x_j} \right] + G_k + G_b - \rho \varepsilon - Y_M + S_k \quad (3.42)$$

$$\frac{\partial}{\partial t}(\rho\varepsilon) + \frac{\partial}{\partial x_j}(\rho\varepsilon u_j) = \frac{\partial}{\partial x_j} \left[ \left( \mu + \frac{\mu_t}{\sigma_\varepsilon} \right) \frac{\partial \varepsilon}{\partial x_j} \right] + \rho C_1 S_\varepsilon - \rho C_2 \frac{\varepsilon^2}{k + \sqrt{\nu \varepsilon}} + C_{1\varepsilon} \frac{\varepsilon}{k} C_{3\varepsilon} G_b + S_\varepsilon \quad (3.43)$$

Where

$$C_1 = \max \left[ 0.43, \frac{\eta}{\eta + 5} \right] \quad (3.44)$$

$$\eta = S \frac{k}{\varepsilon} \quad (3.45)$$

$$S = \sqrt{2 S_{ij} S_{ij}} \quad (3.46)$$

In the above equations,  $G_k$  represents the generation of turbulence kinetic energy due to the mean velocity gradients.  $G_b$  represents the generation of turbulence kinetic energy due to buoyancy.  $Y_M$  represents the effects of compressibility on turbulence.

$C_2$  and  $C_{2\varepsilon}$  are constants.

$\sigma_k$  and  $\sigma_\varepsilon$  are the turbulent Prandtl numbers.

$S_k$  and  $S_\varepsilon$  are user-defined source terms.

As in other  $k-\varepsilon$  models, the eddy viscosity is computed from.

$$\mu_t = \rho C_\mu \frac{k^2}{\varepsilon} \quad (3.47)$$

$$C_\mu = \frac{1}{A_0 + A_s \frac{k u^*}{\varepsilon}} \quad (3.48)$$

$C_\mu$  is the mean strain and rotation rates which has value is 0.09.

$C_{1\varepsilon}$ ,  $\sigma_k$  and  $\sigma\varepsilon$  are constant which have values are 1.44, 1.9 and 1.2.

Where

$$u^* = \sqrt{S_{ij}S_{ij} + \tilde{\Omega}_{ij}\tilde{\Omega}_{ij}} \quad (3.49)$$

$$\tilde{\Omega}_{ij} = \Omega_{ij} - 2\varepsilon_{ijk}\omega_k$$

$\overline{\Omega}_{ij}$  is the mean rate-of-rotation tensor viewed in a moving reference frame with the angular velocity  $\omega_k$ .

$A_0$  and  $A_s$  are constant, they given by

$$A_0 = 4.04.$$

$$A_s = \sqrt{6} \cos\phi . \quad (3.50)$$

$$\phi = \frac{1}{3} \cos^{-1} \left[ \sqrt{6} w \right] \quad (3.51)$$

$$w = \frac{S_{ij}S_{ik}S_{ki}}{S^{03}} \quad (3.52)$$

Where

$$S^0 = \sqrt{S_{ij}S_{ij}} \quad (3.53)$$

$$S_{ij} = \frac{1}{2} \left( \frac{\partial u_j}{\partial x_i} + \frac{\partial u_i}{\partial x_j} \right) \quad (3.54)$$

### 3.4 Boundary Conditions

The governing equations for the flow under consideration are nonlinear partial differential equations. For the solution of these equations, the boundary conditions should also be defined. Boundary conditions are identified as follows. At the duct inlet the flow is assumed that the axial velocity is uniform ( $U$ ), temperature is prescribed  $T_{in}$ , and the turbulent intensity is specified. The turbulent intensity at the inlet is determine form expression given below (ANSYS, Inc., 2018).

$$I = 0.16Re^{-1/8} \quad (3.55)$$

At the duct outlet section, the flow is assumed to be fully developed and temperature variation in the flow direction is negligible. This means that zero normal gradients prevail for all flow variables except for the pressure. For the duct walls, the no-slip condition is applied. A constant heat flux is applied to the top and bottom walls. The back and front walls are insulated. In the present numerical study, the near wall treatment was based on enhanced wall function.

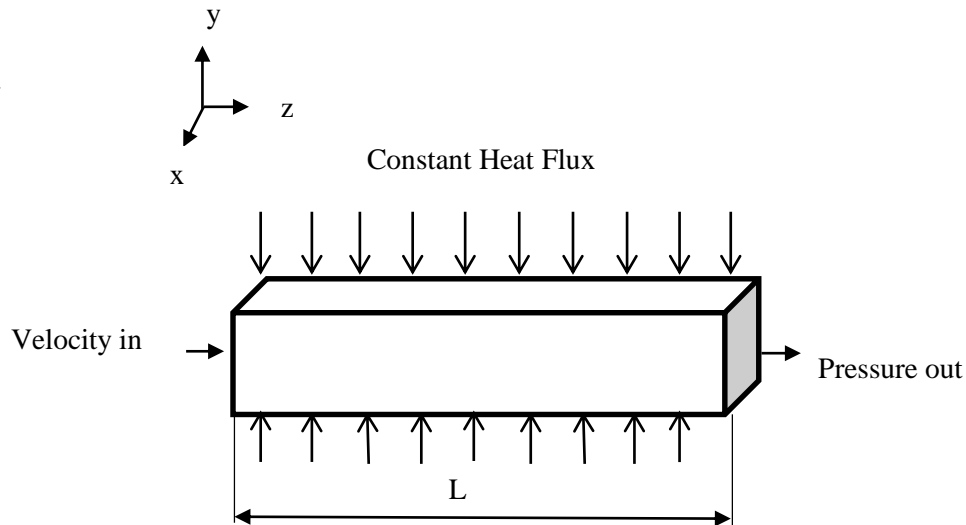


**Figure 2** Geometry and coordinate system of the problem.

### 3.5 Calculation of Mixture Properties

As mentioned above, the flow of nano-particle water mixture is modelled as a single phase flow. Modeling the mixture as single phase flow requires determination of the mixture properties.

**Table 1** Thermo-physical properties for water and Al<sub>2</sub>O<sub>3</sub>, CuO and ZnO.

Property	Basic fluid (water)	Nanoparticle (Al <sub>2</sub> O <sub>3</sub> )	Nanoparticle (CuO)	Nanoparticle (ZnO)
Specific heat $\left(\frac{J}{kg\ K}\right)$	4182	765	533	495.2
Density $\left(\frac{kg}{m^3}\right)$	998.2	3600	6500	5600
Thermal conductivity $\left(\frac{W}{m\ K}\right)$	0.6	36	17.65	13
Viscosity $(Pa\ s)$	$1 \times 10^{-3}$	–	–	–

#### 3.5.1. Density Calculation

The effective density of nanofluid with different particle concentrations is calculated from the expression given below Wang et al (2008).

$$\rho_{nf} = (1 - \phi)\rho_{bf} + \phi\rho_p$$

In this expression,  $\phi$  is particle volume fraction,  $\rho_{bf}$  and  $\rho_p$  are densities of the base fluid and particle, respectively.

For  $\phi = 1\%$ ,  $\rho_{bf} = 998.2 \frac{kg}{m^3}$  and  $\rho_p = 3600 \frac{kg}{m^3}$ , nanofluid density is calculated as

$$\rho_{nf} = (1 - 1 \times 10^{-2}) 998.2 \left( \frac{kg}{m^3} \right) + 1 \times 10^{-2} \times 3600 \left( \frac{kg}{m^3} \right)$$

$$\rho_{nf} = 1024.218 \left( \frac{kg}{m^3} \right)$$

### 3.5.2 Specific Heat

The effective specific heat with different concentrations is calculated from equation Buongiorno et al. (2006) and Zhou et al. (2008).

$$\text{At } \phi = 1\%, (\rho C)_{bf} = 998.2 \frac{kg}{m^3} \times 4182 \frac{J}{kg \text{ K}}, (\rho C)_p = 600 \frac{kg}{m^3} \times 773 \frac{J}{kg \text{ K}}$$

$$\text{and } \rho_{nf} = 1024.218 \frac{kg}{m^3}.$$

$$C_{nf} = \frac{(1 - \phi)(\rho C)_{bf} + \phi(\rho C)_p}{\rho_{nf}}$$

$$C_{nf} = \frac{(1 - 1 \times 10^{-2}) \times 998.2 \frac{kg}{m^3} \times 4182 \frac{J}{kg \text{ K}} + 10^{-2} \times 600 \frac{kg}{m^3} \times 773 \frac{J}{kg \text{ K}}}{1024.218 \frac{kg}{m^3}}$$

$$C_{nf} = 4061.897 \frac{J}{kg \text{ K}}$$

### 3.5.3 Thermal Conductivity

The effective thermal conductivity with different consent ratios is calculated from equation Corcione (2011).

$$\frac{k_{nf}}{k_{bf}} = 1 + 4.4 \text{Re}^{0.4} \text{Pr}^{0.66} \left( \frac{T}{T_{fr}} \right)^{10} * \left( \frac{k_p}{k_{bf}} \right)^{0.03} * \phi^{0.66}$$

At  $\phi = 1\%$

$$k_{nf} \text{ is } 0.631324 \frac{W}{m \text{ K}}$$

### 3.5.4 Viscosity

The effective viscosity  $\mu_{nf}$  with different volume fractions is calculated from equation (Coercion, 2011) .

$$\frac{\mu_{nf}}{\mu_{bf}} = \frac{1}{1 - 34.87 \left( \frac{d_p}{d_f} \right)^{-0.03} \phi^{1.03}}$$

At  $\phi=1\%$

$\mu_{nf}$  is 0.00109 (Pa s)

The above given correlations are collected in Table 2

**Table 2** Correlations used for calculation of nanofluid properties.

Property	Correlation	Reference
Density $\left( \frac{kg}{m^3} \right)$	$\rho_{nf} = (1 - \phi)\rho_{bf} + \phi\rho_p$	Wang et al. (2008)
Specific heat $\left( \frac{J}{kg K} \right)$	$C_{nf} = \frac{(1 - \phi)(\rho C)_{bf} + \phi(\rho C)_p}{\rho_{nf}}$	Buongiorno et al. (2006) and Zhou et al. (2006)
Thermal conductivity $\left( \frac{W}{m K} \right)$	$\frac{k_{nf}}{k_{bf}} = 1 + 4.4Re^{0.4}Pr^{0.66} \left( \frac{T}{T_{fr}} \right)^{10} * \left( \frac{k_p}{k_{bf}} \right)^{0.03} * \phi^{0.66}$	Corcione (2011)
Viscosity (Pa s)	$\frac{\mu_{nf}}{\mu_{bf}} = \frac{1}{1 - 34.87 \left( \frac{d_p}{d_f} \right)^{-0.03} \phi^{1.03}}$	Corcione (2011)

**Table 3** Nanofluid thermo - physical properties with different volume fractions.

Property	Particle volume concentration, $\phi$				
	0.0%	1%	2%	3%	4%
Specific heat $\left(\frac{J}{kg\ K}\right)$	4182	4061.897	3947.744	3839.111	3735.606
Density $\left(\frac{kg}{m^3}\right)$	998.2	1001.0818	1050.236	1076.254	1102.272
Thermal conductivity $\left(\frac{W}{m\ K}\right)$	0.6	0.631324	0.649494	0.66468	0.678205
Viscosity $(Pa\ s)$	$1 \times 10^{-3}$	0.00109	0.001202	0.001342	0.001522

### 3.6. Calculation of Nusselt Number

To calculate Nusselt Number

$$Q = \dot{m}C_p\Delta T \quad (3.56)$$

Where

Q is total heat transfer rate

$\dot{m}$  is mass flow rate.



$\Delta T$  is the difference temperature between output and input in the duct.

$$Q = \dot{m} C_p (T_{out} - T_{in}) \quad (3.57)$$

$$\dot{m} = \rho U A \quad (3.58)$$

$$h = \frac{Q}{A_h (T_w - T_b)} \quad (3.59)$$

$h$  is heat transfer coefficient.

$$h = \frac{\dot{m} C_p (T_{out} - T_{in})}{A_h (T_w - T_b)} \quad (3.60)$$

$$A_h = 2(a.L) \quad (3.61)$$

$A_h$  is the surface area to top and bottom duct.

$$\bar{h} = \frac{\rho A \bar{U} C_p (T_{out} - T_{in})}{2(a.L)(T_w - T_b)} \quad (3.62)$$

$$\overline{Nu} = \frac{\bar{h} D_h}{k} \quad (3.63)$$

### 3.7. Calculation Friction Coefficient

To find friction factor, we write the force balance in fully developed flow in flow direction as follows:

$$\sum F_z = \sum F_{z, \text{pressure}} + \sum F_{z, \text{shear stress}} = 0 \quad (3.64)$$

$$\sum F_{z, \text{pressure}} = -\sum F_{z, \text{shear stress}} \quad (3.65)$$

By multiplying pressure by cross section area, we obtain the pressure force acting on a control volume.

$$\sum F_{z, \text{pressure}} = \Delta p \frac{\pi D_h^2}{4} \quad (3.66)$$

By multiplying shear stress by inner surface area, we obtain the shear force as,

$$\sum F_{z, \text{shear stress}} = -\tau_w \pi D_h L \quad (3.67)$$

Substitute Eq. (3.66) and Eq. (3.67) into Eq. (3.65), we get

$$\Delta p \frac{\pi D_h^2}{4} = \tau_w \pi D_h L \quad (3.68)$$

$$\Delta p = \frac{\tau_w \pi D_h L}{\frac{\pi D_h^2}{4}} = \frac{4 \tau_w \pi D_h L}{\pi D_h^2} \quad (3.69)$$

After arranging Eq. (3.69)

$$\Delta p = \frac{4 \tau_w L}{D_h} \quad (3.70)$$

by dividing both sides of Eq. (3.70) by  $\rho V^2$ , we get

$$\frac{\Delta p}{\rho V^2} = \frac{4 \tau_w L}{\rho V^2 D_h} = \frac{1}{2} \frac{L}{D_h} \left( \frac{8 \tau_w}{\rho V^2} \right) \quad (3.71)$$

Noting that

$f = \left( \frac{8 \tau_w}{\rho V^2} \right)$  is the friction factor Darcy friction factor ( $f$ ), then we can rewrite Eq. (3.71)

as,

$$\Delta p = f \frac{\rho V^2}{2} \frac{L}{D_h}$$

To calculate the friction factor  $f$ , shear stress is calculated from the simulated velocity distribution using the following expression,

$$\tau_{total \ shear \ stress} = (\mu_{laminar} + \mu_{turbulent}) \frac{d\bar{w}}{dy} \quad (3.72)$$

## **CHAPTER IV**

### **NUMERICAL SOLUTION**

In the present study, the computational fluid dynamics (CFD) software combined with the finite volume method is employed to solve the nonlinear governing equations (Eqs. (3-21), (3-32), (3-41), (3-42) and (3-43)) of turbulent nano fluid forced convection heat transfer in a duct. For this, ANSYS-FLUENT software package is utilized. A brief explanation about ANSYS is given below.

#### **4.1 ANSYS PROGRAM**

ANSYS is general purpose software, used to simulate problems in the area of physics, structure, vibration, fluid dynamics, heat transfer, electromagnetic, etc. It has ability to simulate test or working conditions, in virtual environment before manufacturing prototypes of products. (Abas, 2013). FLUENT is a computer program which has been used extensively in fluid flow simulation under complex geometries using the finite volume method. Detailed information of fluid temperature, velocity components, pressure and turbulence intensity within the flow domain can be simulated (Li, 2015).

The control-volume-based technique is used to convert a general scalar transport equation into a set of algebraic equations that can be solved numerically. Integration of the governing equations on the individual control volumes yields linear algebraic equations for the discrete dependent variables (unknowns) such as velocities, pressure and temperature. The solution of the resulting linear equation systems gives updated values of the dependent variables.

## 4.2 Finite Volume Differencing Schemes

For the finite volume methods (FMV), the domain is divided up into a number of control volumes, with the value at the center of the control volume being held to be representative for the value over the entire control volume. By integrating the original PDE over the control volume, the equation is cast into a form that ensures conservation.

Governing equations of a general convection-diffusion problem can be described by following general partial differential equation

$$\frac{\partial}{\partial t}(\rho\phi) + \nabla \cdot (\rho \mathbf{u} \phi) = \nabla \cdot (\Gamma \nabla \phi) + S \quad (4.1)$$

Where  $\Gamma$  is the diffusion coefficient.

$S$  is any source term for the scalar  $\phi$  per unit volume.

$\rho$  is the density fluid.

$\mathbf{u}$  is the fluid velocity field.

In The Eq. (4.1), the first term is the time derivative and it is the rate of change of  $\phi$  with respect to time, and the second term is the advection component and it is the transport of  $\phi$  by the ambient velocity field. On the right hand side of the Eq. (4.1), the first term is the transport due to diffusion, whilst the last term is the contribution due to sources of  $\phi$  within the field.

For a three-dimensional domain Equation (4.1) can be written as

$$\frac{\partial}{\partial t}(\rho\phi) + \frac{\partial}{\partial x}(\rho u \phi) + \frac{\partial}{\partial y}(\rho v \phi) + \frac{\partial}{\partial z}(\rho w \phi) = \frac{\partial}{\partial x} \left( \Gamma \frac{\partial \phi}{\partial x} \right) + \frac{\partial}{\partial y} \left( \Gamma \frac{\partial \phi}{\partial y} \right) + \frac{\partial}{\partial z} \left( \Gamma \frac{\partial \phi}{\partial z} \right) + S \quad (4.2)$$

$u, v$  and  $w$  being the  $x, y$  and  $z$  components of the velocity, respectively. For the steady transport equation, the time derivative is zero, and the Eq. (4.2) can be written:

$$\frac{\partial}{\partial x}(\rho u \phi) + \frac{\partial}{\partial y}(\rho v \phi) + \frac{\partial}{\partial z}(\rho w \phi) = \frac{\partial}{\partial x} \left( \Gamma \frac{\partial \phi}{\partial x} \right) + \frac{\partial}{\partial y} \left( \Gamma \frac{\partial \phi}{\partial y} \right) + \frac{\partial}{\partial z} \left( \Gamma \frac{\partial \phi}{\partial z} \right) + S \quad (4.3)$$

The finite volume discretization of the three-dimensional steady transport equation, given in Eq. (4.3), is found by integrating the equation over the control volume shown in Figure 3.

$$\begin{aligned} & \int_b^t \int_s^n \int_w^e \frac{\partial}{\partial x}(\rho u \phi) dx dy dz + \int_b^t \int_s^n \int_w^e \frac{\partial}{\partial y}(\rho v \phi) dx dy dz + \int_b^t \int_s^n \int_w^e \frac{\partial}{\partial z}(\rho w \phi) dx dy dz = \\ & \int_b^t \int_s^n \int_w^e \frac{\partial}{\partial x} \left( \Gamma \frac{\partial \phi}{\partial x} \right) dx dy dz + \int_b^t \int_s^n \int_w^e \frac{\partial}{\partial y} \left( \Gamma \frac{\partial \phi}{\partial y} \right) dx dy dz + \int_b^t \int_s^n \int_w^e \frac{\partial}{\partial z} \left( \Gamma \frac{\partial \phi}{\partial z} \right) dx dy dz \\ & + \int_b^t \int_s^n \int_w^e S dx dy dz \end{aligned} \quad (4.4)$$

The derivatives at face of control volumes can be approximated with central differences and linear interpolation. The resulting equations can be written as linear algebraic equations as below (Patankar, 1980).

$$a_P \phi_P = a_E \phi_E + a_W \phi_W + a_N \phi_N + a_S \phi_S + a_T \phi_T + a_B \phi_B + b \quad (4.5)$$

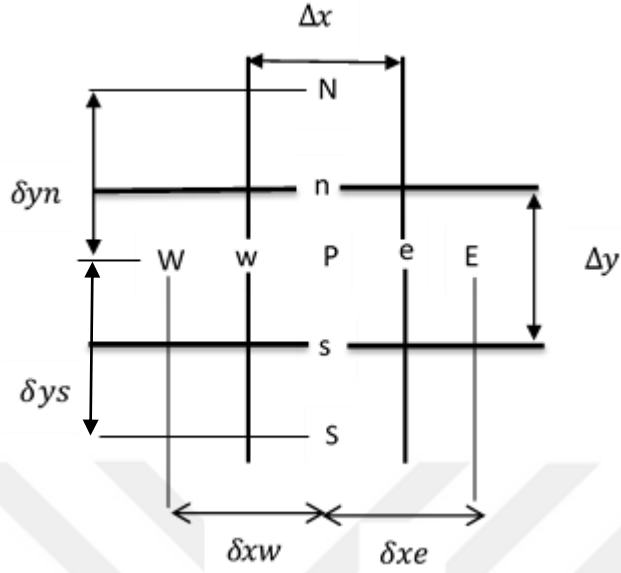


**Figure 3** The geometry for a single control volume in a two -dimensional Cartesian mesh

Where

$$a_E = D_e A (|P_e|) + F_e, 0 \quad (4.6)$$

$$a_W = D_w A (|P_w|) + F_w, 0 \quad (4.7)$$

$$a_N = D_n A (|P_n|) + F_n, 0 \quad (3.8)$$

$$a_S = D_s A (|P_s|) + F_s, 0 \quad (4.9)$$

$$a_T = D_t A (|P_t|) + F_t, 0 \quad (4.10)$$

$$a_B = D_b A (|P_b|) + F_b, 0 \quad (4.11)$$

$$ap^0 = \frac{\rho p^0 \Delta x \Delta y \Delta z}{\Delta t} \quad (4.12)$$

$$b = S_c \Delta x \Delta y \Delta z + ap^0 \phi p^0 \quad (4.13)$$

$$ap = a_E + a_W + a_N + a_S + a_T + a_B + ap^0 - Sp \Delta x \Delta y \Delta z \quad (4.14)$$

In these expressions,  $F$ 's are mass flow rates across the control volume faces,  $D$ 's are diffusion coefficients across the control faces and  $P$ 's are Peclet numbers (the ratio of  $F$  to  $D$ ,  $P=F/D$ ) at the control volume faces.  $F$ 's represent the strength of the convection;  $D$ 's represent the strength diffusion. The function  $A(|P|)$  varies depending on the discretization scheme. It is given for different scheme in Table 4.

The flow rates are

$$F_e = (\rho u)_e \Delta y \Delta z \quad (4.15)$$

$$F_w = (\rho u)_w \Delta y \Delta z \quad (4.16)$$

$$F_n = (\rho u)_n \Delta z \Delta x \quad (4.17)$$

$$F_s = (\rho u)_s \Delta z \Delta x \quad (4.18)$$

$$F_t = (\rho u)_t \Delta x \Delta y \quad (4.19)$$

$$F_b = (\rho u)_b \Delta x \Delta y \quad (4.20)$$

The conductances are

$$D_e = \frac{\Gamma_e \Delta y \Delta z}{(\delta x)_e} \quad (4.21)$$

$$D_w = \frac{\Gamma_e \Delta y \Delta z}{(\delta x)_w} \quad (4.22)$$

$$D_n = \frac{\Gamma_n \Delta z \Delta x}{(\delta y)_n} \quad (4.23)$$

$$D_s = \frac{\Gamma_s \Delta z \Delta x}{(\delta y)_s} \quad (4.24)$$

$$D_t = \frac{\Gamma_t \Delta x \Delta y}{(\delta z)_t} \quad (4.25)$$

$$D_b = \frac{\Gamma_b \Delta x \Delta y}{(\delta z)_b} \quad (4.26)$$

**Table 4** Finite volume differencing schemes.

Scheme	Formula for $A( P )$
1-Central difference	$1 - 0.5( P )$
2-Upwind	1
3-hybrid	$\max(0, 1 - 0.5( P ))$
4-power law	$\max(0, (1 - 0.1 P )^5)$
5-exponential (exact)	$ P  / [\exp( P ) - 1]$

### 4.3 Numerical Simulation

A computational fluid dynamic technique (CFD) and the finite volume method were combined to solve the governing equations (3-21), (3-32), (3-41), (3-42) and (3-43)) of turbulent flow in a square cross-section duct with a constant heat flux. The control volume



in the domain is employed to discretize the scalar transport equations and obtain sets of algebraic equation which can be solved numerically (ANSYS Inc, 2019).

The numerical simulation is used at various Reynolds numbers and different concentrations (1, 2, 3 and 4%). Different size of nanoparticles diameter is used in simulation. The finite volume formulation and semi-implicit method for pressure-linked equations algorithm are used to solve the discretized equations derived from the partial nonlinear differential equations of the mathematical model. The convection terms of the transport equations are discretized by the second-order upwind scheme. Through the calculation, the residuals of the algebraic discretized equations, resulting from the spatial integration of the conservation equations over finite control volumes, are monitored. All calculations in program are considered to be converged when the residuals for all discretized equations are smaller than  $10^{-6}$ .

#### **4.3.1 Number of Iterations and Convergence**

For obtaining the converged solutions, the residuals were carefully monitored. Figure 4 displays the residuals monitor history. As seen in this figure, the residuals of all the variables become less than  $10^{-6}$  around 1000 iteration.

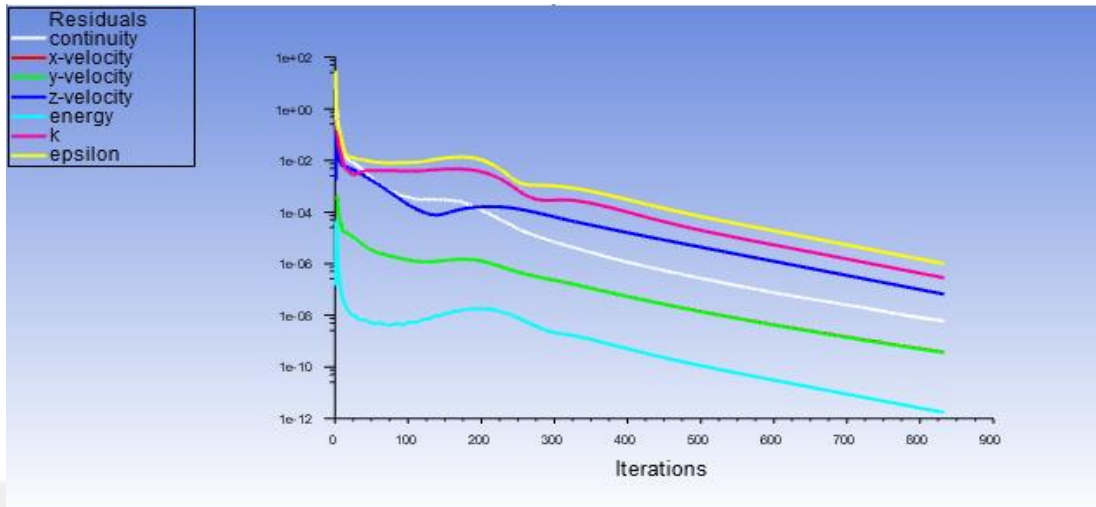


**Figure 4** Number of iterations and residual monitors.

#### 4.4 Grid Independence Analysis and Validation of Numerical Results.

Figure 5 shows the geometry used in the simulations. For the validation test, flow of pure water was considered. The duct is 0.7 m long and cross section is  $1 \times 1 \text{ cm}^2$  square. A constant heat flux of  $q=10 \text{ kW/m}^2$  is supplied to the top and bottom surfaces of the channel.

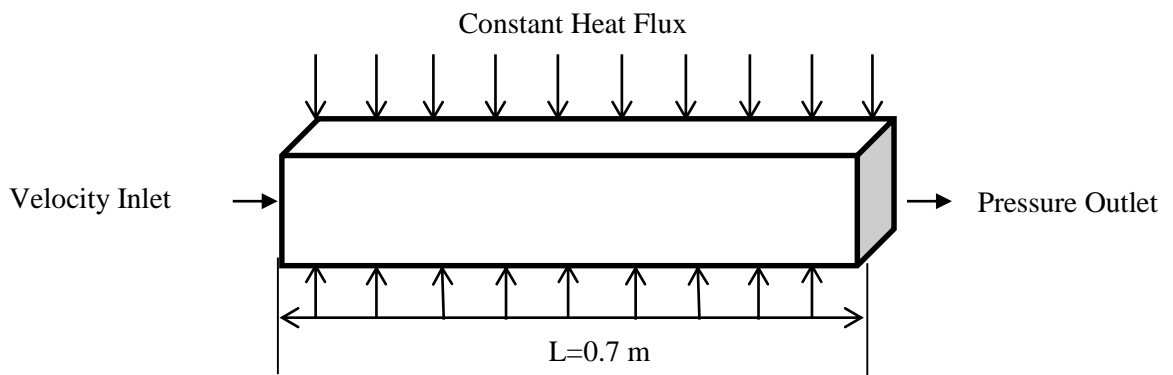


**Figure 5** Geometry test for pure water

In the beginning, for the grid independence analysis, an extensive testing was carried out with different non-uniform mesh systems. For this purpose, the number of mesh densities (60×60×300), (70×70×300), and (80×80×3000) were tested and the results were compared with each other. Moreover, to check the accuracy and reliability of the formulation and CFD technique used in the study, the results obtained by the CFD simulations are compared with the results obtained from empirical correlation Dittus-Boelter equation given by Eq. (4.27) Bergman et al. (2011), for the Nusselt number vs the Reynold number for pure water.

$$Nu = 0.023 Re^{0.8} Pr^{0.4} \quad (4.27)$$

Figure 6 illustrates the variation of Nusselt number obtained from simulations with different meshes, from correlation (Eq. 4.27) and results from the article by Ajeel et al. (2017). For these results water is taken as the working fluid. The numerical results are taken from the fully developed region of the duct. The results of the present CFD analysis with grid systems considered show good agreement with the empirical correlation and results of Ajeel et al. (2017). Therefore, in this study, the number of grid points in the x, y, and z-directions are set to (60×60×300) and considered as the optimum mesh size and shown in Fig. 7.

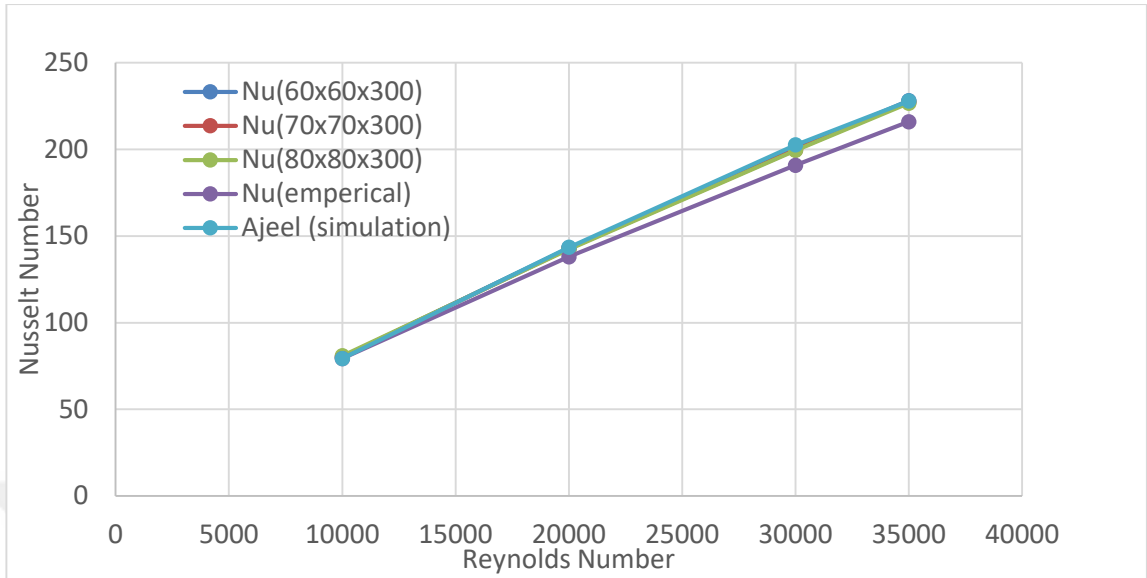


**Figure 6** Variation of Nusselt number with Reynolds number at different mesh densities for pure water , empirical correlation and Ajeel et al .(2017).

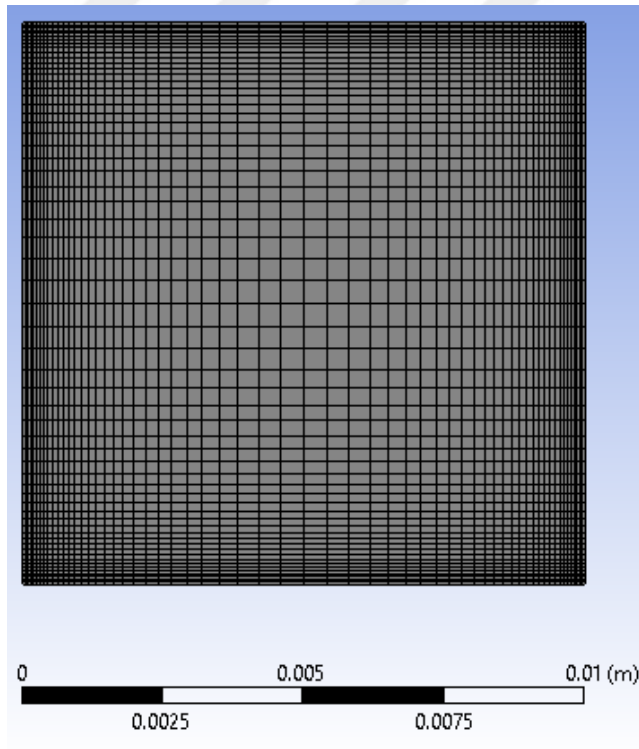


**Figure 7** Grid distribution of square cross section duct.

For pure water, Darcy friction factor obtained from the present numerical simulations and from Blasius correlation (White, 1991) are compared in Fig. 8.

$$f = 4C_f = 4(0.0791 \text{Re}^{-\frac{1}{4}}) \quad (4.28)$$

**Table 5** Friction factor for different Reynolds number.

Reynold Number	Friction Factor
10000	0.031
20000	0.026
30000	0.024
35000	0.0231

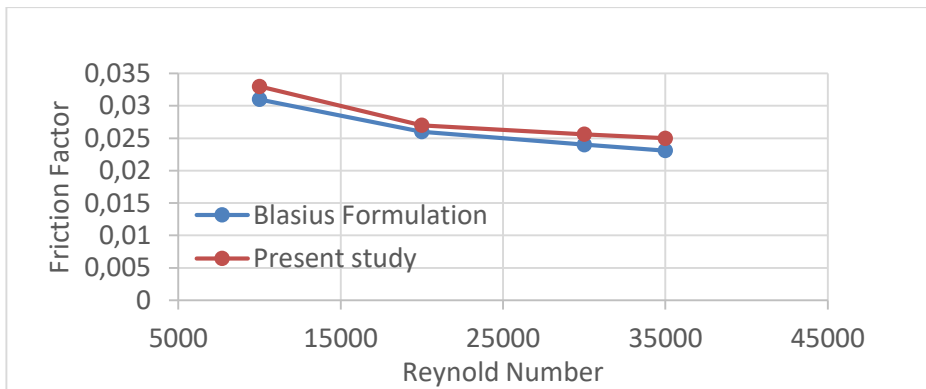


**Figure 8** Comparison of friction coefficients obtained from Blasius formulation and present study.

#### 4.5 Validation Study for Nanofluids

To check the validity of the results obtained for nanofluids, the study carried out by Kaya et al. (2015) considered and computations are performed for different Reynolds number

with mixture of water and  $\text{Al}_2\text{O}_3$  at volume fraction of  $\phi=0.03$ . Heat transfer coefficients are compared in Figure 9. As seen in Figure 9, the results of the present study and the study by Kaya et al. (2015) are very close to each other. Based on the comparisons given in Figures 6, 8 and 9, we conclude that the mathematical formulation and the numerical technique used in the present study yield valid results.

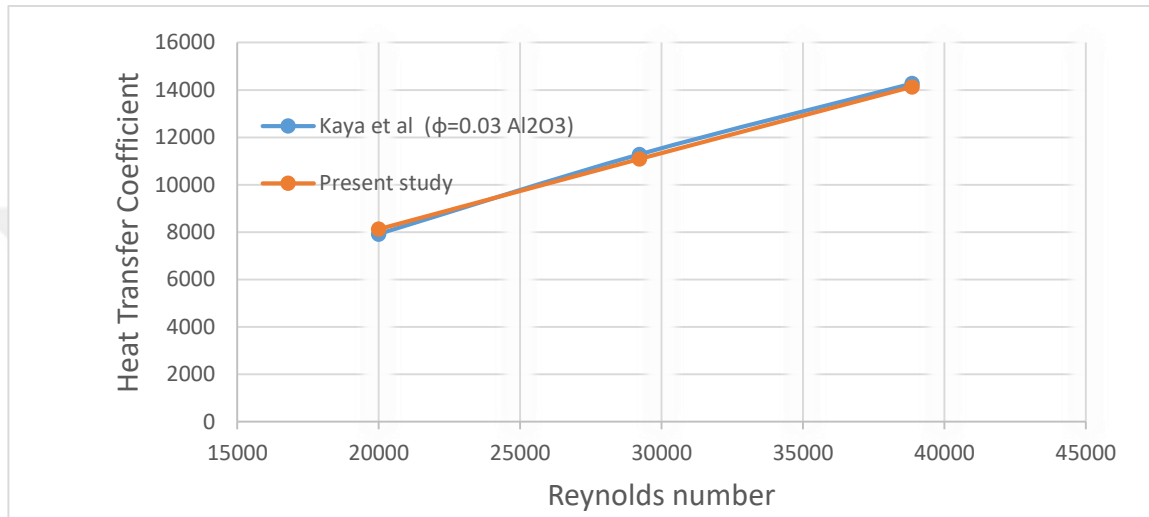


**Figure 9** Comparison of the present result with results of Kaya et al. (2015) for nanofluids  $\text{Al}_2\text{O}_3$  – water at  $\phi=0.03$

## CHAPTER V

### RESULTS AND DISCUSSION

In this chapter, the results of the numerical simulations are presented and discussed. For the simulations, the geometry shown in Fig.10 is considered. As nano particles  $\text{Al}_2\text{O}_3$ ,  $\text{CuO}$  and  $\text{ZnO}$  are used. Effects of volume fraction, particle diameter, Reynolds number and particle material on the heat transfer coefficient and friction coefficient were investigated. The nano particle volume fraction was changed between 0.01-0.04%, diameter of the particles was changed between 30-53 nm, Reynolds number was changed between 10000 and 35000.

#### 5.1 Geometry of Problem

Figure 10 shows the geometry used in the simulations. It is 1 m long and cross section is square of  $1 \times 1 \text{ cm}^2$  area. A constant heat flux  $q=10 \text{ kW/m}^2$  is supplied to the top and bottom surfaces of the channel, front and back surfaces are insulation.

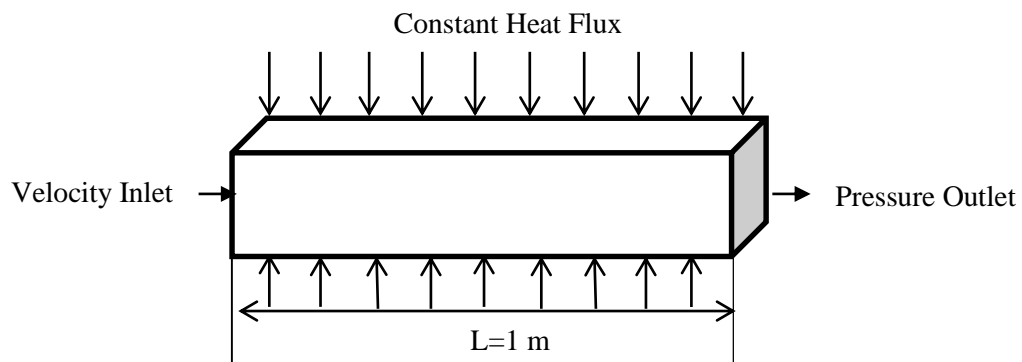


**Figure 10** Geometry study of the problem.

## 5.2 The Effect of Nanoparticle Concentration on Heat Transfer

To analyze the effects of the nanoparticle volume fraction on heat transfer rate, the simulations were carried out for  $\text{Al}_2\text{O}_3$ -water mixture with volume fractions  $\phi=1, 2, 3$  and 4% at different Reynolds numbers. For all these calculations, the particle diameter is kept at 30 nm. The Nusselt numbers obtained from the numerical result are compared in Figure 11. In this figure, the Nusselt number of the pure water case is also included. As seen in this figure, Nusselt number increases with the increasing volume fraction at all Reynolds numbers considered. It is also observed that the increase in Nusselt number with volume fraction increase is more pronounced at higher Reynolds numbers. This increase is due to the high thermal conductivity of nanoparticles and the strong motion of nanoparticles.

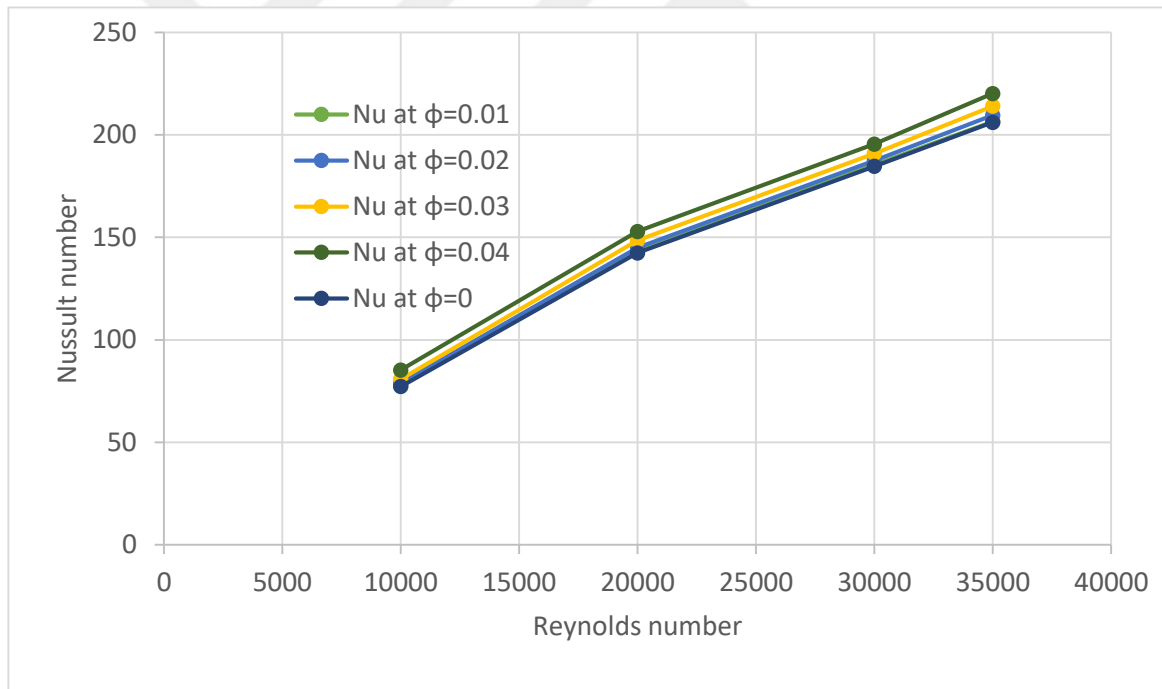


**Figure 11** Variation of Nusselt number with Reynolds number and volume fraction for  $\text{Al}_2\text{O}_3$ - water mixture.

## 5.3 The Effect of Nanoparticle Diameter on the Heat Transfer

To analyze the effects of the nanoparticle diameter on the heat transfer rate, the simulations were carried out for  $\text{Al}_2\text{O}_3$ -water mixture with particle diameters  $d=30, 45$



and 53 nm at different Reynolds numbers. For all these calculations, the particle volume fraction is kept at 4%. The Nusselt numbers obtained from the numerical result are plotted in Figure 12. In this figure, the Nusselt number of the pure water case is also included. As seen in this figure, Nusselt number decrease with the increasing diameter at all Reynolds number. It is seen that this decrease is very small. The particle size effects can be explained as reducing nanoparticle size the surface area per unit volume decrease. Since heat transfer is dependent on the surface area, heat transfer decreases. In Fig. 12, the nanofluid with 30 nm nanoparticle diameter has the highest Nusselt number, whereas, the nanoparticle with a diameter of 53 nm has the lowest Nusselt number. However, as seen the effects of the particle size on the heat transfer is very small in the range considered in this study.

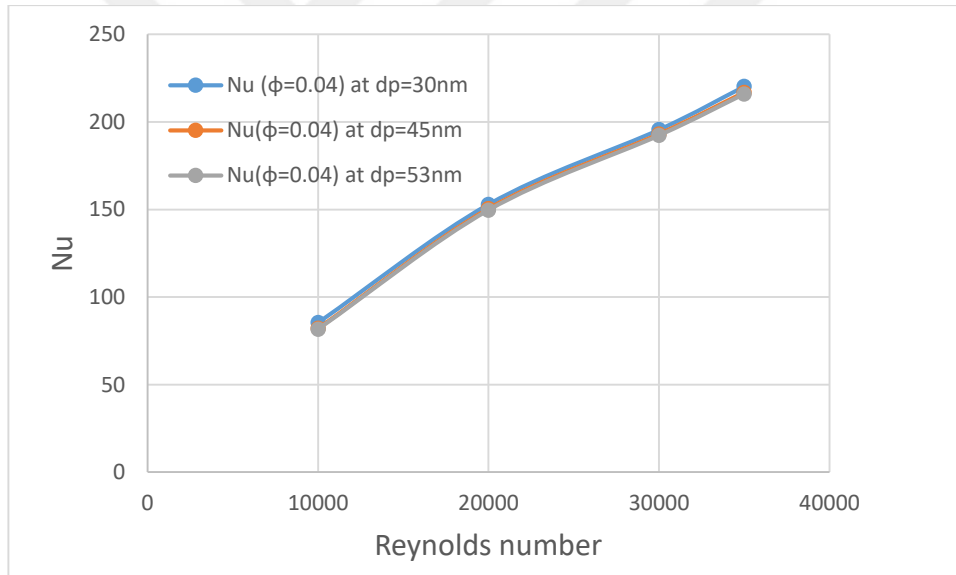


**Figure 12** Variation of Nusselt number with Reynolds number at different nanoparticle diameters for  $\text{Al}_2\text{O}_3$ -water mixture.

#### 5.4 The Effect of Nano Particle Type on Nusselt Number

To investigate the effects of the nanoparticle type on the Nusselt number, simulations were carried out for different nano particles ( $\text{Al}_2\text{O}_3$ , CuO and ZnO)- water mixture at volume fraction 4% at different Reynolds numbers from (10000 to 35000). For all these calculations, the particle volume fraction is kept at 4%. The Nusselt numbers obtained for different nano particle-water mixture are plotted in Figure 13. In this figure, the Nusselt number of the pure water case is also included. As seen in the figure, Nusselt number is

increasing with increasing Reynolds number. It is seen also that Nusselt number for (Al<sub>2</sub>O<sub>3</sub>-water) mixture is higher compared with Nusselt numbers for nanofluids of CuO and ZnO) and pure water.

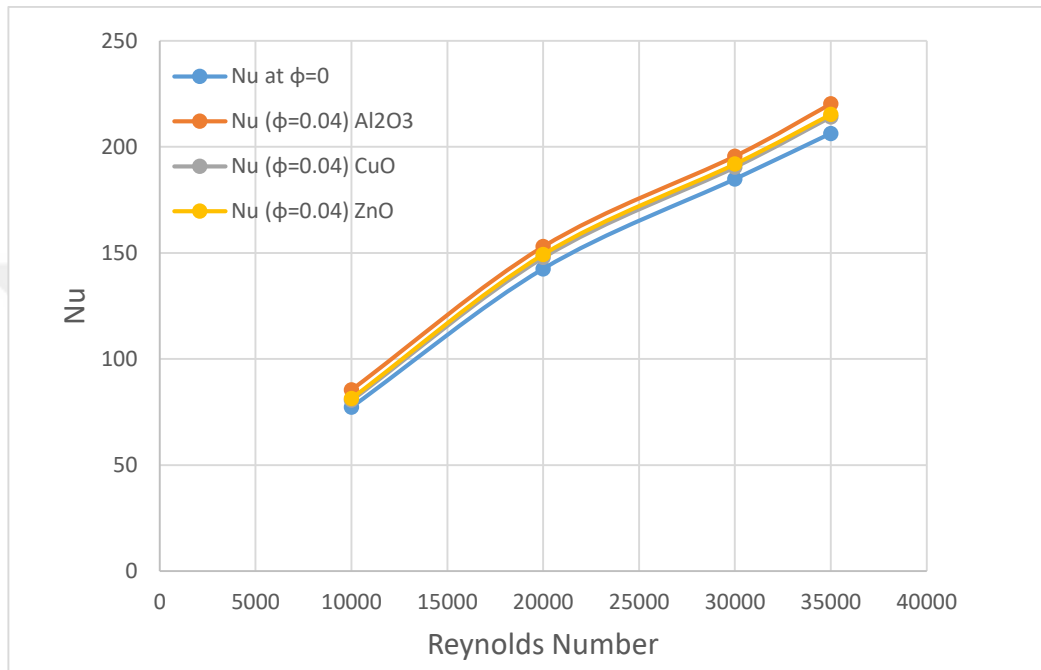


**Figure 13** Variation of Nusselt number with Reynolds number for different nanoparticles (Al<sub>2</sub>O<sub>3</sub>, CuO and ZnO) - water mixtures at volume fraction 4% .

### 5.5 Variation of the Heat Transfer Coefficient

To investigate the effects of the nanoparticle type on the heat transfer coefficient, the simulations were carried out for different nano particles Al<sub>2</sub>O<sub>3</sub>- water mixture at volume fraction 4%, with particle diameters  $d=30$  nm for all nano particles in simulations, at different Reynolds numbers from (10000 to 35000). For all these calculations, the particle volume fraction is kept at 4%. The heat transfer coefficient is plotted in Figure14. In this figure, the heat transfer coefficient of the pure water case is also included. As seen in this figure, the Heat transfer coefficient is increasing by increasing Reynolds number. It is seen also that Heat transfer coefficient at (Al<sub>2</sub>O<sub>3</sub>-water) mixture is higher compared with pure water.

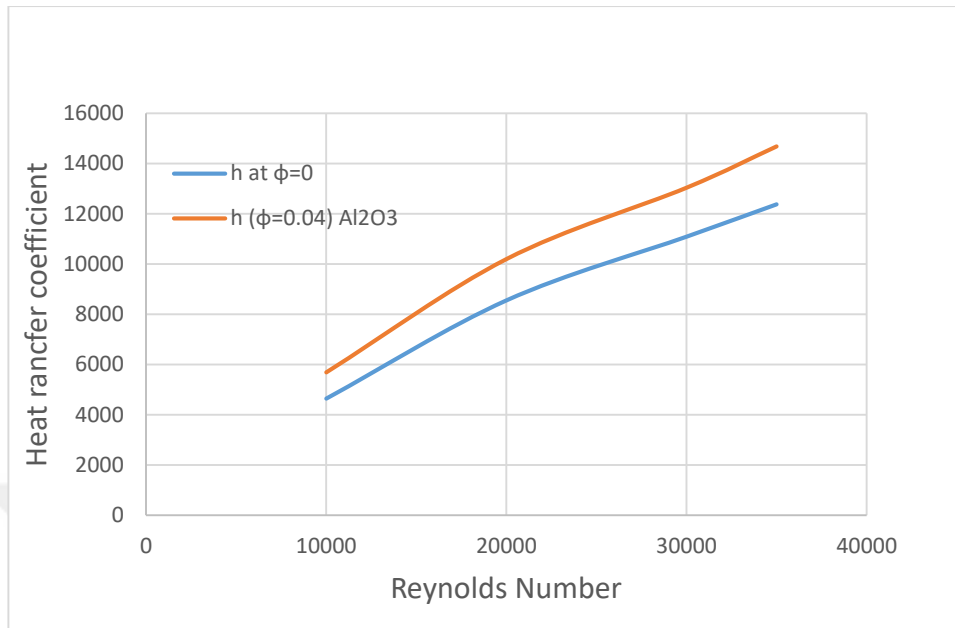


**Figure 14** Variation of heat transfer coefficient with Reynolds number for pure water and Al<sub>2</sub>O<sub>3</sub> - water mixture at volume fraction 4 % .

### 5.6 The Effect of Nanoparticles Type on Wall Shear Stress

The variation of the wall shear stress for pure water, and Al<sub>2</sub>O<sub>3</sub> and CuO nanoparticle mixtures along the channel at Reynolds number 35000 and  $\phi=4\%$  is plotted in Fig 15. It can be seen in this figure that the wall shear stress variation for Al<sub>2</sub>O<sub>3</sub> and CuO nanoparticle mixtures are very close to each other. However, wall shear stress with nanofluids is higher than pure water flow. This variation is due to the effective dynamic viscosity for different types of nanofluids and pure water.

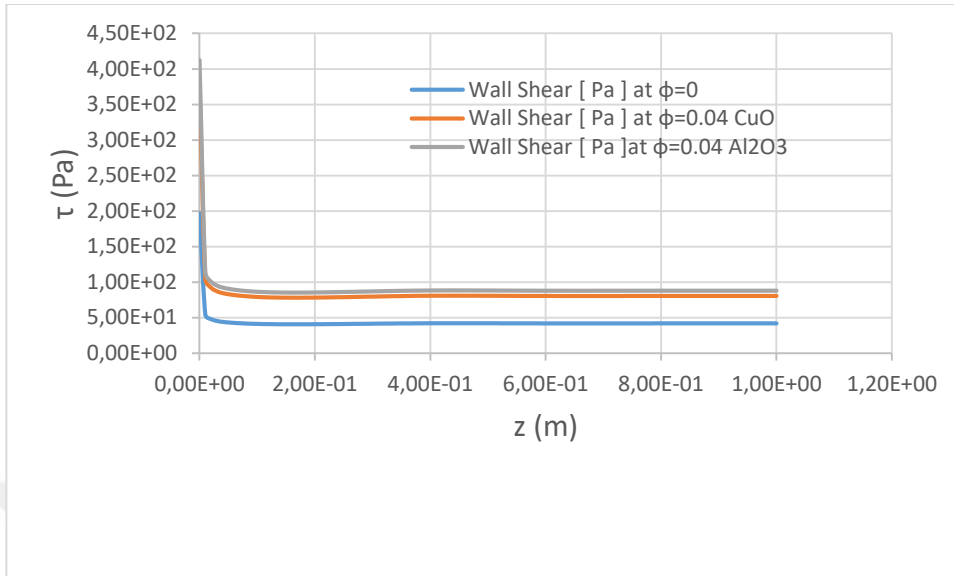


**Figure 15** Variation of shear stress with Reynolds number for different nanofluids (Al<sub>2</sub>O<sub>3</sub> and CuO)- water mixture at volume fraction of 4%.

### 5.7 The Effect of Volume Fraction on Wall Shear Stress

Figure 16 shows the variation of the shear stress along the channel with different volume fractions at Reynolds number of 35000 for pure water and Al<sub>2</sub>O<sub>3</sub> mixture nanofluid. It is seen in this figure that the shear stress for pure water is less than for nanofluids. It is also seen in this figure that the shear stress increases with increases volume fraction.

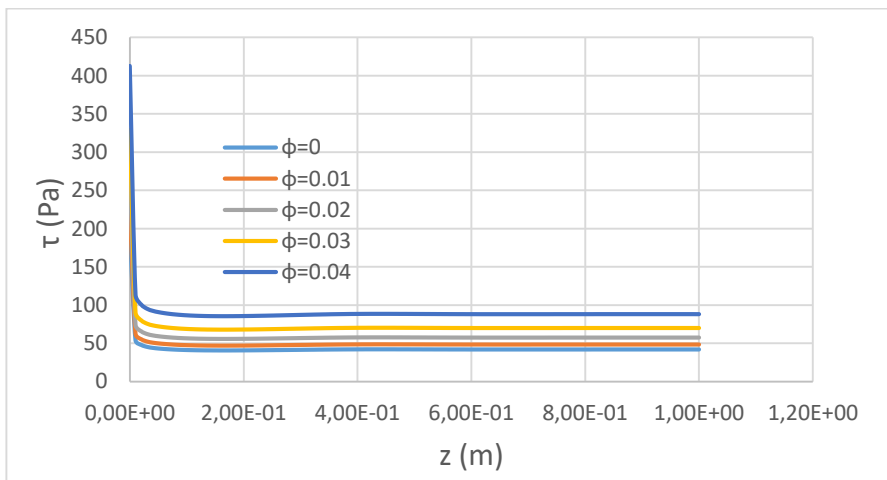


**Figure 16** Variation of shear stress along the channel for pure water and nonfluid Al<sub>2</sub>O<sub>3</sub> of volume fraction from 1-4% at Reynolds number of 35000.

## CHAPTER VI

### CONCLUSION

#### 6.1 Summary

In Chapter 1, some general information is presented about the characteristics nanofluids. Advantages of using suspended solid nanoparticles in a base fluid like water and oil are analyzed. Summarize of studies found in the literature about the nanofluid flow and heat transfer is also given in Chapter 1. Effects of the volume concentration, particle diameter and shape on heat transfer coefficient are reviewed.

In Chapter 2, the thermo physical properties of the nanofluids such as density, specific heat, thermal conductivity and viscosity were explained in detail. All-important correlations used for the calculation of the physical properties of nanofluids were summarized. The observations for all thermo physical properties were briefly discussed.

In Chapter 3, firstly the problem in our study has been described, the kind of base fluid and nano particles are explained. The single phase and multi-phase models were described. Secondly, the governing equations of the problem (continuity, momentum, and energy equations) were given. The turbulence model used in the simulations was formulated and described briefly. The mixture physical properties were calculated using the correlation given in Chapter 2. Finally, the boundary conditions were described for inlet and outlet duct and top, bottom, back and front surfaces.

In Chapter 4, the numerical approach used for the analysis forced convection heat transfer was described. After giving a short description of ANSYS-FLUENT software package, the mesh independency and the validation study were presented by comparing numerical results with the experimental and numerical results from the literature. The correlations

exist in the literature for pure fluids were also used for validation of the results of the present study.

In Chapter 5, results of the numerical analysis performed for  $\text{Al}_2\text{O}_3/\text{water}$ ,  $\text{CuO}/\text{water}$  and  $\text{ZnO}/\text{water}$  nanofluid inside a straight square duct under constant wall heat flux were presented. Effects of Reynolds number, particle volume fraction, and particle size and particle material on heat transfer enhancement were investigated.

## 6.2 Conclusions

The thermophysical properties of nanofluids has important effects on the analysis and evaluation of performance heat transfer estimation approaches. The density and specific heat parameters can be accurately predicted using the mixtures and thermal equilibrium models. However, thermal conductivity and viscosity values for nanofluids cannot be easily predicted. Some models for thermal conductivity are explored and it is seen that nano particle diameter, nanoparticle volumetric fraction and temperature are the most important parameters. It is observed that Corcione model for thermal conductivity and viscosity is the most accurate model for calculation of these nanofluid properties.

In the present study, it is seen that aluminum oxide ( $\text{Al}_2\text{O}_3$ ) is the best nanoparticle material compared with other materials since it has higher thermal conductivity. It was observed that heat transfer rate in the duct increases with the increasing Reynolds number, increasing volume fraction, and with the decreasing particle size. However, with increasing volume fraction, wall friction coefficient also increases.

## 6.3 Future Work

- As explained in Chapter 2, there are different expressions for the determination of thermo-physical properties of the nanofluids and they may yield different results. Hence, a detailed study may be carried out using different expressions for the determination of the physical properties of nanofluids.

- Ethylene glycol have high thermal conductivity and viscosity compared with other base fluids such as water and oil. Due to these properties (thermal conductivity and the viscosity), nano particle-ethylene glycol mixture may have different flow and heat transfer characteristics. Hence, it would be important to carry out analysis for ethylene glycol based nanofluids.



## REFERENCES

Abas, M. F. (2013). *Determination of airflow characteristics for a set of stabilizer and elevator using simulation software* (Doctoral dissertation, Universiti Tun Hussein Onn Malaysia).

Abdolbaqi, M. K., Azwadi, C. S. N., & Mamat, R. (2014). Heat transfer augmentation in the straight channel by using nanofluids. *Case Studies in Thermal Engineering*, 3, 59-67.

Ajeel, R. K., & Salim, W. S. I. W. (2017, September). A CFD study on turbulent forced convection flow of Al<sub>2</sub>O<sub>3</sub>-water nanofluid in semi-circular corrugated channel. In *IOP Conference Series: Materials Science and Engineering* (Vol. 243, No. 1, p. 012020). IOP Publishing.

ANSYS, Inc. (2018), "ANSYS Fluent User's Guide, Release 19.0", Equation (6.68)

Batchelor, G. K. (1977). The effect of Brownian motion on the bulk stress in a suspension of spherical particles. *Journal of fluid mechanics*, 83(1), 97-117.

Bergman, T. L., Incropera, F. P., Lavine, A. S., & Dewitt, D. P. (2011). *Introduction to heat transfer*. John Wiley & Sons.

Brinkman, H. C. (1952). The viscosity of concentrated suspensions and solutions. *The Journal of Chemical Physics*, 20(4), 571-571.

Bruggeman, V. D. (1935). Berechnung verschiedener physikalischer Konstanten von heterogenen Substanzen. I. Dielektrizitätskonstanten und Leitfähigkeiten der Mischkörper aus isotropen Substanzen. *Annalen der physik*, 416(7), 636-664.



Buongiorno, J. (2006). Convective transport in nanofluids. *Journal of heat transfer*, 128(3), 240-250.

Corcione, M. (2011). Empirical correlating equations for predicting the effective thermal conductivity and dynamic viscosity of nanofluids. *Energy Conversion and Management*, 52(1), 789-793.

Choi, S. U., & Eastman, J. A. (1995). Enhancing thermal conductivity of fluids with nanoparticles (No. ANL/MSD/CP--84938; CONF-951135--29). *Argonne National Lab., IL (United States)*.

Eastman, J. A. (1999). Novel thermal properties of nanostructured materials (No. ANL/MSD/CP-96711). *Argonne National Lab., IL (US)*.

Ebrahimnia-Bajestan, E., Niazmand, H., Duangthongsuk, W., & Wongwises, S. (2011). Numerical investigation of effective parameters in convective heat transfer of nanofluids flowing under a laminar flow regime. *International Journal of Heat and Mass Transfer*, 54(19-20), 4376-4388.

Einstein, A. (1906). Eine neue bestimmung der moleküldimensionen. *Annalen der Physik*, 324(2), 289-306.

Ghiaasiaan, S. M. Convective heat and mass transfer. 2011.

Hamilton, R. L., & Crosser, O. K. (1962). Thermal conductivity of heterogeneous two-component systems. *Industrial & Engineering chemistry fundamentals*, 1(3), 187-191.

Heris, S. Z., Esfahany, M. N., & Etemad, G. (2007). Numerical investigation of nanofluid laminar convective heat transfer through a circular tube. *Numerical Heat Transfer, Part A: Applications*, 52(11), 1043-1058.

Heris, S. Z., Etemad, S. G., & Esfahany, M. N. (2006). Experimental investigation of oxide nanofluids laminar flow convective heat transfer. *International Communications in Heat and Mass Transfer*, 33(4), 529-535.

Hwang, Y. J., Ahn, Y. C., Shin, H. S., Lee, C. G., Kim, G. T., Park, H. S., & Lee, J. K. (2006). Investigation on characteristics of thermal conductivity enhancement of nanofluids. *Current Applied Physics*, 6(6), 1068-1071.

Kaya, O. (2015). Numerical Investigation of Heat Transfer, Pressure Drop and Wall Shear Stress Characteristics of Al<sub>2</sub>O<sub>3</sub>-Water Nanofluid in a Square Duct. *Arabian Journal for Science and Engineering*, 40(12), 3641-3655.

Keblinski, P., Phillpot, S. R., Choi, S. U. S., & Eastman, J. A. (2002). Mechanisms of heat flow in suspensions of nano-sized particles (nanofluids). *International journal of heat and mass transfer*, 45(4), 855-863.

Krieger, I. M., & Dougherty, T. J. (1959). A mechanism for non-Newtonian flow in suspensions of rigid spheres. *Transactions of the Society of Rheology*, 3(1), 137-152.

Li, N. (2015). Comparison between three different CFD software and numerical simulation of an ambulance hall.

Mahbubul, I. M., Saidur, R., & Amalina, M. A. (2012). Latest developments on the viscosity of nanofluids. *International Journal of Heat and Mass Transfer*, 55(4), 874-885.

Maxwell, J. C. (1881). A treatise on electricity and magnetism (Vol. 1). Clarendon press.

Minakov, A. V., Guzei, D. V., Pryazhnikov, M. I., Zhigarev, V. A., & Rudyak, V. Y. (2016). Study of turbulent heat transfer of the nanofluids in a cylindrical channel. *International Journal of Heat and Mass Transfer*, 102, 745-755.

Mirmasoumi, S., & Behzadmehr, A. (2008). Effect of nanoparticles mean diameter on mixed convection heat transfer of a nanofluid in a horizontal tube. *International Journal of Heat and Fluid Flow*, 29(2), 557-566.

Mohammed, H. A., Bhaskaran, G., Shuaib, N. H., & Abu-Mulaweh, H. I. (2011). Influence of nanofluids on parallel flow square microchannel heat exchanger performance. *International Communications in Heat and Mass Transfer*, 38(1), 1-9.

Namburu, P. K., Das, D. K., Tanguturi, K. M., & Vajjha, R. S. (2009). Numerical study

of turbulent flow and heat transfer characteristics of nanofluids considering variable properties. *International journal of thermal sciences*, 48(2), 290-302.

Nielsen, L. E. (1970). Generalized equation for the elastic moduli of composite materials. *Journal of Applied Physics*, 41(11), 4626-4627.

O'Hanley, H., Buongiorno, J., McKrell, T., & Hu, L. W. (2012). Measurement and model validation of nanofluid specific heat capacity with differential scanning calorimetry. *Advances in Mechanical Engineering*, 4, 181079.

Patankar, S. (1980). *Numerical heat transfer and fluid flow*. CRC press.

Schwartz, L. M., Garboczi, E. J., & Bentz, D. P. (1995). Interfacial transport in porous media: Application to dc electrical conductivity of mortars. *Journal of Applied Physics*, 78(10), 5898-5908.

Shih, T. H., Liou, W. W., Shabbir, A., Yang, Z., & Zhu, J. (1995). A new k- $\epsilon$  eddy viscosity model for high reynolds number turbulent flows. *Computers & Fluids*, 24(3), 227-238.

Ting, H. H., & Hou, S. S. (2015). Investigation of laminar convective heat transfer for Al<sub>2</sub>O<sub>3</sub>-water nanofluids flowing through a square cross-section duct with a constant heat flux. *Materials*, 8(8), 5321-5335.

Xuan, Y., & Roetzel, W. (2000). Conceptions for heat transfer correlation of nanofluids. *International Journal of heat and Mass transfer*, 43(19), 3701-3707.

Wang, X. Q., & Mujumdar, A. S. (2008). A review on nanofluids-part I: theoretical and numerical investigations. *Brazilian Journal of Chemical Engineering*, 25(4), 613-630.

Wen, D., & Ding, Y. (2004). Experimental investigation into convective heat transfer of nanofluids at the entrance region under laminar flow conditions. *International journal of heat and mass transfer*, 47(24), 5181-5188.

White, F.M. (1991), *Viscous Fluid Flow*, 2nd ed., McGraw Hill, New York, NY.

Yarmand, H., Gharekhani, S., Kazi, S. N., Sadeghinezhad, E., & Safaei, M. R. (2014). Numerical investigation of heat transfer enhancement in a rectangular heated pipe for turbulent nanofluid. *The Scientific World Journal*, 2014.

Yu, W., & Choi, S. U. S. (2003). The role of interfacial layers in the enhanced thermal conductivity of nanofluids: a renovated Maxwell model. *Journal of nanoparticle research*, 5(1-2), 167-171.

Zhou, S. Q., & Ni, R. (2008). Measurement of the specific heat capacity of water-based Al<sub>2</sub>O<sub>3</sub> nanofluid. *Applied Physics Letters*, 92(9), 093123.